Bimodal regulation of an Elk subfamily K⁺ channel by phosphatidylinositol 4,5-bisphosphate

Xiaofan Li,[1,2] Andriy Anishkin,[3] Hansi Liu,[1] Damian B. van Rossum,[1,2] Sree V. Chintapalli,[4,5] Jessica K. Sassic,[1] David Gallegos,[1] Kendra Pivaroff-Ward,[6] and Timothy Jegla[1,2]

[1]Department of Biology and [2]Huck Institutes of the Life Sciences, Pennsylvania State University, University Park, PA 16802
[3]Department of Biology, University of Maryland, College Park, MD 20742
[4]Arkansas Children's Nutrition Center and [5]Department of Pediatrics, University of Arkansas for Medical Sciences, Little Rock, AR 72202
[6]Department of Earth and Space Sciences, University of Washington, Seattle, WA 98195

Phosphatidylinositol 4,5-bisphosphate (PIP$_2$) regulates Shaker K⁺ channels and voltage-gated Ca²⁺ channels in a bimodal fashion by inhibiting voltage activation while stabilizing open channels. Bimodal regulation is conserved in hyperpolarization-activated cyclic nucleotide–gated (HCN) channels, but voltage activation is enhanced while the open channel state is destabilized. The proposed sites of PIP$_2$ regulation in these channels include the voltage-sensor domain (VSD) and conserved regions of the proximal cytoplasmic C terminus. Relatively little is known about PIP$_2$ regulation of Ether-á-go-go (EAG) channels, a metazoan-specific family of K⁺ channels that includes three gene subfamilies, Eag (Kv10), Erg (Kv11), and Elk (Kv12). We examined PIP$_2$ regulation of the Elk subfamily potassium channel human Elk1 to determine whether bimodal regulation is conserved within the EAG K⁺ channel family. Open-state stabilization by PIP$_2$ has been observed in human Erg1, but the proposed site of regulation in the distal C terminus is not conserved among EAG family channels. We show that PIP$_2$ strongly inhibits voltage activation of Elk1 but also stabilizes the open state. This stabilization produces slow deactivation and a mode shift in voltage gating after activation. However, removal of PIP$_2$ has the net effect of enhancing Elk1 activation. R347 in the linker between the VSD and pore (S4–S5 linker) and R479 near the S6 activation gate are required for PIP$_2$ to inhibit voltage activation. The ability of PIP$_2$ to stabilize the open state also requires these residues, suggesting an overlap in sites central to the opposing effects of PIP$_2$ on channel gating. Open-state stabilization in Elk1 requires the N-terminal eag domain (PAS domain + Cap), and PIP$_2$-dependent stabilization is enhanced by a conserved basic residue (K5) in the Cap. Our data shows that PIP$_2$ can bimodally regulate voltage gating in EAG family channels, as has been proposed for Shaker and HCN channels. PIP$_2$ regulation appears fundamentally different for Elk and KCNQ channels, suggesting that, although both channel types can regulate action potential threshold in neurons, they are not functionally redundant.

INTRODUCTION

Phosphatidylinositol 4,5-bisphosphate (PIP$_2$) is a regulator of a wide variety of ion channels, including evolutionarily diverse members of the voltage-gated cation channel superfamily (Hilgemann et al., 2001; Suh and Hille, 2008; Rodríguez-Menchaca et al., 2012b; Zhou and Logothetis, 2013). PIP$_2$ is found in the inner membrane leaflet where its negatively charged headgroup is ideally positioned to interact with the gating machinery of voltage-gated ion channels. This machinery includes the activation gate of the channel pore and the S4–S5 linker, which couples the voltage-sensor domain (VSD) to that gate (Long et al., 2005a). In KCNQ K⁺ channels, PIP$_2$ is required to couple voltage-sensor movement to

pore opening and interacts with positively charged residues in the S4–S5 linker and immediately downstream of the S6 activation gate (Zaydman et al., 2013). In contrast, the Shaker channel Kv1.2 is dually modulated: PIP$_2$ inhibits voltage activation but also increases maximal currents, suggesting open-state stabilization (Rodriguez-Menchaca et al., 2012a). Interactions between the S4–S5 linker of Kv1.2 and PIP$_2$ inhibit voltage activation by restricting outward movement of the voltage sensor (Rodriguez-Menchaca et al., 2012a), but sites involved in PIP$_2$-dependent enhancement have not been identified. However, some voltage-gated Ca²⁺ channels show the same dual modulation by PIP$_2$ (Wu et al., 2002; Suh et al., 2010), and a residue at the intracellular face of the domain III S6 has been shown to regulate PIP$_2$-dependent current enhancement (Zhen et al., 2006).

Correspondence to Timothy Jegla: tjj3@psu.edu

Bimodal modulation of gating by PIP$_2$ has also been observed for the sea urchin hyperpolarization-activated CNG (HCN) channel SpIH (Flynn and Zagotta, 2011), which belongs to a separate superfamily of voltage-gated cation channels that share a cytoplasmic cyclic nucleotide–binding domain (CNBD). This CNBD superfamily includes HCN channels, CNG channels, and Ether-á-go-go (EAG) family voltage-gated K$^+$ channels in animals (Yu and Catterall, 2004; Jegla et al., 2009), as well as K$^+$ channels in plants (Schachtman et al., 1992; Sentenac et al., 1992), ciliate protozoans (Jegla and Salkoff, 1994, 1995), and prokaryotes (Brams et al., 2014). In SpIH, PIP$_2$ depolarizes the voltage activation range as in Shaker (Flynn and Zagotta, 2011), but this enhances rather than inhibits activation in the physiological range because SpIH is opened by hyperpolarization. The site of action was localized to the transmembrane channel core, but specific residues were not identified. PIP$_2$ also reduces maximal SpIH current, and this opposing inhibitory effect depends on basic residues in the C-linker, which connects the cytoplasmic CNBD to the activation gate (Flynn and Zagotta, 2011). The C-linker has been shown to play a critical role in the gating of HCN and CNG channels (Decher et al., 2004; Craven and Zagotta, 2006). CNG channels are also inhibited by phosphatidylinositol 3,4,5-bisphosphate (PIP$_3$; Womack et al., 2000; Zhainazarov et al., 2004; Bright et al., 2007), although identified sites of action appear to be in the proximal N terminus and distal C terminus outside the conserved channel core domains (Brady et al., 2006; Dai et al., 2013).

Much less is known about PIP$_2$-dependent modulation of EAG family K$^+$ channels. These channels can be identified by a unique subunit structure and separate into three gene subfamilies, Eag (Kv10), Erg (Kv11), and Elk (Kv12), based on sequence conservation (Warmke and Ganetzky, 1994; Ganetzky et al., 1999). The EAG family is ancient but metazoan specific. The EAG subunit structure appears to have arisen in basal metazoans, and the Eag, Erg, and Elk subfamilies first appeared and functionally differentiated in a common ancestor of cnidarians and bilaterians (Martinson et al., 2014; Li et al., 2015b). Virtually all data on PIP$_2$ modulation of the EAG channel family comes from a single gene, the human Erg subfamily channel Erg1 (hErg1, Kv11.1), which underlies the I$_{Kr}$ current critical to cardiac action potential repolarization (Sanguinetti et al., 1995; Trudeau et al., 1995; Keating and Sanguinetti, 2001). The application of exogenous PIP$_2$ enhances hErg1 activation (Bian et al., 2001, 2004), and depletion of native PIP$_2$ causes a small reduction in hErg1 currents (Kruse and Hille, 2013). The effect of PIP$_2$ on Eag and Elk subfamily channel gating has not yet been described, and bimodal modulation by PIP$_2$ has not been observed for the EAG family.

The EAG channel family subunit domain structure consists of a typical voltage-gated K$^+$ channel core, a C-linker/cyclic nucleotide–binding homology domain (CNBHD) structurally equivalent to the C-linker/CNBD gating domain of HCN and CNG channels (Brelidze et al., 2012), and a unique N-terminal eag domain consisting of a Per-Arndt-Sim (PAS) domain (Morais Cabral et al., 1998) with an EAG channel–specific Cap (Gustina and Trudeau, 2012). The CNBHD receives its designation as a homology domain because although structurally similar to CNBD, it appears self-liganded in crystal structures (Brelidze et al., 2012, 2013), and EAG family channels do not appear to respond to the application of intracellular cyclic nucleotides (Brelidze et al., 2009, 2012). The eag domain docks on the CNBHD (Gianulis et al., 2013; Haitin et al., 2013), and in hErg1 it stabilizes open channels, producing the characteristic slow deactivation of hErg1 (Morais Cabral et al., 1998; Wang et al., 1998). This time-dependent open-state stabilization causes deactivation to occur in a more hyperpolarized voltage range than activation, a phenomenon that has been referred to as "mode shift" (Alonso-Ron et al., 2008; Villalba-Galea et al., 2008; Tan et al., 2012; Hull et al., 2014; Goodchild et al., 2015). Deletion of the eag domain or Cap in hErg1 reduces open-state stabilization and therefore speeds deactivation and diminishes mode shift (Morais Cabral et al., 1998; Wang et al., 1998; Alonso-Ron et al., 2008; Muskett et al., 2011; Tan et al., 2012; Hull et al., 2014; Goodchild et al., 2015). The N-terminal of the Cap of hErg1 is highly conserved and forms an amphipathic helix by NMR; neutralization of conserved basic residues within the helix speeds deactivation (Muskett et al., 2011). The location of the N-terminal of the Cap is not resolved in EAG family crystals (Morais Cabral et al., 1998; Haitin et al., 2013), but it has been proposed to interact directly with the channel core (Wang et al., 1998) or alternatively with the CNBHD (Haitin et al., 2013). Interestingly, the proposed site of PIP$_2$ interaction with hErg1 is a cluster of positive charges in the C terminus downstream of the CNBHD (Bian et al., 2004) in an area that is poorly conserved even within the Erg channel subfamily, and thus it is not clear how PIP$_2$ might regulate other EAG family channels.

We examined PIP$_2$ regulation of the human Elk family channel Elk1 (HsElk1, Kv12.1) to gain a broader understanding of how PIP$_2$ influences the activity of EAG family channels. We also examined the role of the eag domain in Elk channel gating to see if it plays a functionally equivalent role to what has been observed for hErg1, or inhibits activation and inactivation as has been proposed for the mammalian Eag subfamily channel Eag1 (Kv10.1; Terlau et al., 1997). Elk channels, including Elk1, characteristically have a hyperpolarized voltage-activation range with significant activation at neuronal resting potentials (Trudeau et al., 1999; Zou et al., 2003; Zhang et al., 2010; Li et al., 2015b). Elk2, like the KCNQ-encoded M current, contributes to subthreshold K$^+$ current in hippocampal pyramidal neurons, and genetic or

pharmacologic block of either channel causes hyperexcitability and epilepsy (Peters et al., 2005; Zhang et al., 2010). Comparing how Elk and KCNQ channels differ in terms of PIP_2 regulation is therefore important for determining the degree to which these channels are functionally redundant or occupy separate physiological niches. We chose Elk1 for this study because it is the only mammalian Elk channel that expresses at high enough levels in heterologous systems to enable excised patch recording for direct PIP_2 application.

The results we present here show that the eag domain of Elk1 is functionally equivalent to that of hErg1, and that PIP_2 regulates Elk1 in a bimodal fashion, as has been observed for Shaker, HCN, and calcium channels. PIP_2-dependent regulation of Elk1 requires basic residues in the S4–S5 linker (R347), proximal to the S6 activation gate (R479), and in the Cap of the eag domain (K5).

MATERIALS AND METHODS

Molecular biology
Human Elk1 (Kv12.1, KCNH8) was amplified from whole brain RNA by standard RT-PCR techniques and cloned into the pOX plasmid (Jegla and Salkoff, 1997) for expression in *Xenopus laevis* oocytes. The WT clone used for these studies encodes a channel identical in amino acid sequence to the channel protein encoded
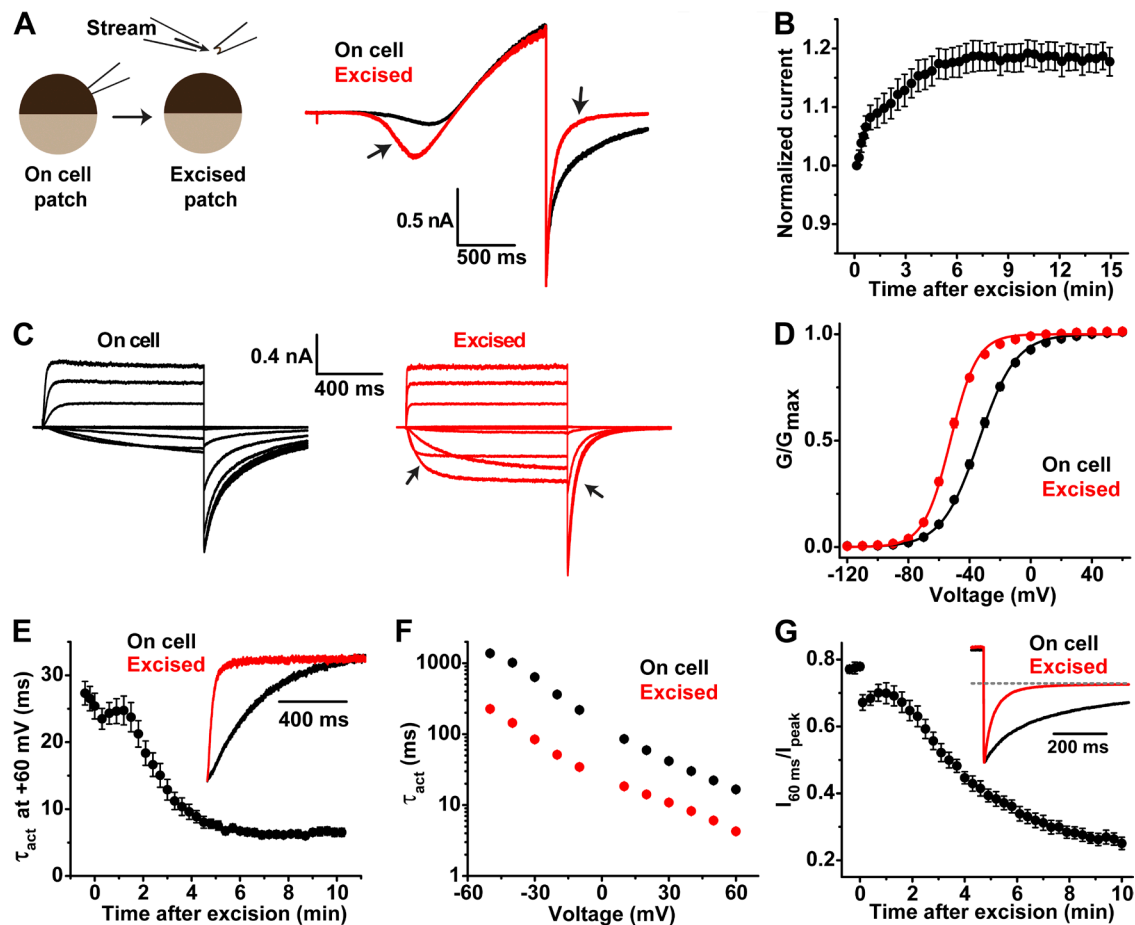

Figure 1. Patch excision alters voltage gating of Elk1. (A) Schematic drawing of on-cell and excised inside-out recording configurations. Currents recorded in response to a 2-s voltage ramp (−120 to 80 mV; −100-mV holding potential) are shown for the on-cell (black) and excised (red) configurations, with high K^+ in the pipette. Arrows point to the increased inward current at hyperpolarized voltages and the rapid deactivation that gradually occur upon patch excision. (B) Peak tail current amplitude at −100 mV (from ramp recordings as in A) increases upon excision and stabilizes within 5–10 min. Data ($n = 8$) were normalized to the first sweep after excision. (C) Elk1 currents recorded in response to a series of 1-s voltage steps (−120 to 60 mV in 20-mV increments; −100-mV holding potential) on cell and after excision and stabilization. Note the fast activation and deactivation in the excised recording (arrows). (D) On-cell and excised G-V curves for Elk1. Data were measured from isochronal tail currents recorded at −100 mV after 1-s steps to the indicated voltages ($n = 32$ and 37, respectively). Curves show single Boltzmann fits of the data (V_{50} and s reported in Table 1). (E) Elk1 activation time constants measured at 60 mV before and after excision. Activation rate speeds up and stabilizes by 6–8 min after excision ($n = 13$); the inset compares normalized current traces recorded at −20 mV (polarity flipped for display purposes). (F) Comparison of on-cell ($n = 15$) and excised ($n = 26$) activation time constants at various voltages. (G) Deactivation kinetics for Elk1 on cell and excised as measured by the fractional tail current amplitude 60 ms after repolarization to −100 mV (lower value = faster deactivation; $n = 8$). (Inset) Normalized tail currents at −100 mV after 2-s prepulse to 60 mV (dotted line, zero current). Data in all panels show mean ± SEM.

by GenBank accession number NM_144633. Mutations and truncations were incorporated via standard oligo-mediated PCR mutagenesis techniques and sequence verified. *Ciona intestinalis* VSP (CiVSP) was provided by J. Cui (Washington University, St. Louis, MO). Expression plasmids were linearized and used as templates for capped cRNA synthesis with the T3 mMessage mMachine kit (Life Technologies). RNA transcripts were purified by LiCl precipitation and rinsed with ice-cold 70% ethanol. Air-dried pellets were dissolved in an appropriate volume of nuclease-free water supplemented with RNase inhibitor SUPERase-In (Life Technologies) and stored at −80°C until use.

Xenopus oocyte preparation, injection, and culture
Xenopus ovaries were obtained from either Xenopus 1 or Nasco. Oocytes were isolated from the ovaries and de-folliculated with 1 mg/ml Type II collagenase (Sigma-Aldrich) in Ca^{2+}-free ND98 (98 mM NaCl, 2 mM KCl, 2 mM $CaCl_2$, 1 mM $MgCl_2$, and 5 mM HEPES, pH 7.2). Snipping the ovaries with scissors to increase fluid access to the interior and pre-rinsing in Ca^{2+}-free ND98 increased the speed of ovary digestion and the quality of oocytes obtained. After digestion, mature, high quality oocytes were transferred into culture solution that included the addition of 1.8 mM Ca^{2+}, 2.5 mM Na-pyruvate, 100 U/ml penicillin, and 100 µg/ml streptomycin to the ND98 base solution. Oocytes were cultured in this solution at 18°C before and after injection. Oocytes were injected with 50–70 nl of RNA solution using a Nanoject II injector (Drummond Scientific Company) and cultured 1–5 d before recording. The amount of RNA injected was adjusted to optimize current size based on empirical observations and varied between constructs. Chemical reagents for solutions were obtained from Sigma-Aldrich.

Patch-clamp recordings
Oocytes were placed in a hypertonic stripping solution (culture solution supplemented with 200 mM sucrose) for 3–10 min to allow separation of the plasma membrane from the vitelline envelope. Forceps were used to remove the vitelline envelopes, and oocytes were transferred to the recording dish filled with internal solution (142 mM K^+, 138 mM methanesulfonate, 4 mM Cl^-, 10 mM HEPES, and 5 mM EGTA, pH 7.2). Patch pipettes were coated with Sticky Wax (Kerr Dental Laboratory Products) to minimize capacitance and had a resistance of 0.4–1 MΩ after fire polishing. The pipette solution contained 142 mM K^+, 1 mM Mg^+, 0.2 mM Ca^{2+}, 140 mM methanesulfonate, 4.4 mM Cl^-, and 10 mM HEPES, pH 7.2. The Ag-AgCl ground was placed in 1 M NaCl and connected to the bath with a 1-M NaCl agarose bridge. Junction potential was cancelled before patch formation, and pipette capacitance was compensated. Inside-out patches were immediately moved into a focal stream of internal solution after excision and maintained under constant perfusion. Data were collected using a Multiclamp 700A amplifier and the pClamp 9 acquisition suite (Molecular Devices). Data were sampled at 20 kHz and filtered at 1.4 kHz. In some cases, multiple sweeps were averaged to improve the signal-to-noise ratio. Phosphatidylinositol-4,5-bisphosphate C-8 (diC8-PIP_2), phosphatidylinositol-4-phosphate C-8 (diC8-PI(4)P), and phosphatidylinositol-3,4,5-trisphosphate C-8 (diC8-PIP_3) were purchased from Cayman Chemicals. 2.5-mM stock solutions were made with internal solution and stored at −80°C. The phosphoinositides were diluted to final concentrations with internal solution and applied directly to the intracellular face of excised patches through the perfusion stream.

Data analysis
G-V curves were determined from isochronal tail currents at −100 mV. Data were fitted with a single Boltzmann distribution in Origin 8.1 (OriginLab) using the equation $f(V) = (A_1 − A_2)/(1 + e^{(V−V50)/s}) + A_2$, where V_{50} represents the midpoint; s is the slope factor; and A_1 and A_2 represent the upper and lower asymptotes, respectively. Data from individual patches were normalized and averaged before plotting, and the Boltzmann fits shown in the figures are simulated using the arithmetic means of V_{50} and s values. For measurements of activation time course, the major phase of current activation (initial 80% of current rise after sigmoidal delay) was fitted with a single exponential in Clampfit (Molecular Devices) using the equation $f(t) = y_0 + Ae^{−t/\tau}$, where y_0 is the current offset, A is the amplitude, and τ is the time constant. Data for dose–response relationships were fit in Origin 8.1 with the modified

TABLE 1

Elk1 Boltzmann fit parameters for standard G-V curves measured from a −100-mV hold

Channel	Parameter	On cell			Excised			10 µM PIP₂		
		Mean	SEM	n[a]	Mean	SEM	n	Mean	SEM	n
WT	V_{50}[b]	−33.9	1.1	32	−52.5	0.8	37	−30.8	0.8	37
	s[c]	12.1	0.2	32	8.7	0.1	37	10.2	0.1	37
Δ2-136	V_{50}	−8.1	1.8	15	−45.2	1.0	15	−13.7	0.8	14
	s	10.1	0.3	15	8.0	0.3	15	8.4	0.3	14
K5Q	V_{50}	−22.6	1.2	9	−55.9	1.3	9	−26.1	1.3	8
	s	9.7	0.2	9	8.2	0.0	9	8.7	0.2	8
R347E	V_{50}	−45.2	2.3	18	−46.4	2.2	18	−25.8	2.9	15
	s	16.4	0.3	18	14.1	0.2	18	16.2	0.4	15
R347C	V_{50}	−20.6	2.4	17	−26.4	1.7	17	−3.5	1.8	12
	s	12.1	0.3	17	13.3	0.3	17	14.3	0.4	12
R475E	V_{50}	−38.5	1.6	17	−37.5	1.0	20	−25.1	1.4	17
	s	12.9	0.4	17	11.4	0.2	20	12.2	0.2	17
R479E	V_{50}	−59.6	2.3	17	−38.3	1.3	20	−43.0	2.0	14
	s	14.4	0.5	17	13.1	0.2	20	15.9	0.4	14
R479Q	V_{50}	−53.7	2.8	11	−47.6	1.8	12	−42.5	2.5	11
	s	14.9	0.3	11	10.4	0.2	12	14.2	0.4	11

[a]n, number of measurements.
[b]V_{50}, Half-maximal activation voltage, mV.
[c]s, slope factor, mV.

Hill equation with an offset: $y = START + (END - START)x^n/(k^n + x^n)$, where START and END are the bottom and top of the curve, respectively; k is the PIP_2 concentration producing half-maximal effect; and n is the Hill coefficient. Statistical significances were assessed using two-tailed Student's t tests.

RESULTS

Patch excision alters voltage-dependent gating of Elk1

We first characterized gating changes that occur in Elk1 after excision of inside-out patches from *Xenopus* oocytes to assess the potential for the existence of PIP_2-dependent regulation. Patch excision leads to gradual loss of PIP_2 from the plasma membrane, and gating alterations that accompany patch excision therefore can reflect PIP_2 dependence. For instance, rundown of KCNQ channels in inside-out patches can be reduced by manipulations that slow the loss of PIP_2 and can be reversed by the application of a soluble PIP_2 analogue diC8-PIP_2 to the intracellular face of the patch (Li et al., 2005; Zaydman et al., 2013). Fig. 1 A shows Elk1 currents in symmetrical K^+ evoked by voltage ramps before patch excision and several minutes after patch excision when

currents had stabilized. Two obvious changes (arrows) include the enhanced activation of Elk1 at hyperpolarized potentials and a dramatic speed up of deactivation. Channel activity as measured by peak tail current at -100 mV after the voltage ramp increased for several minutes after excision and then remained stable through 15 min (Fig. 1 B). Example Elk1 current traces recorded in response to 1-s voltage steps from on-cell and excised patches are shown in Fig. 1 C, and voltage activation (G-V) curves measured from isochronal tail currents are shown in Fig. 1 D (fit parameters are provided in Table 1). Patch excision shifts the V_{50} of the voltage-activation curve -18.6 ± 1.3 mV. It leads to an increase in the activation rate of Elk1 (Fig. 1 E), as measured by a decrease in the time constant of activation (τ_{act}) (Fig. 1, E and F) that occurred over several minutes in parallel with the run-up of tail current size. Patch excision also increases the rate of deactivation, as measured by a significant decrease in the fraction of tail current remaining 60 ms after repolarization from 60 to -100 mV (Fig. 1 G). Measurements of channel activity in excised patches described later in this paper were taken only after currents elicited by voltage ramps had stabilized.
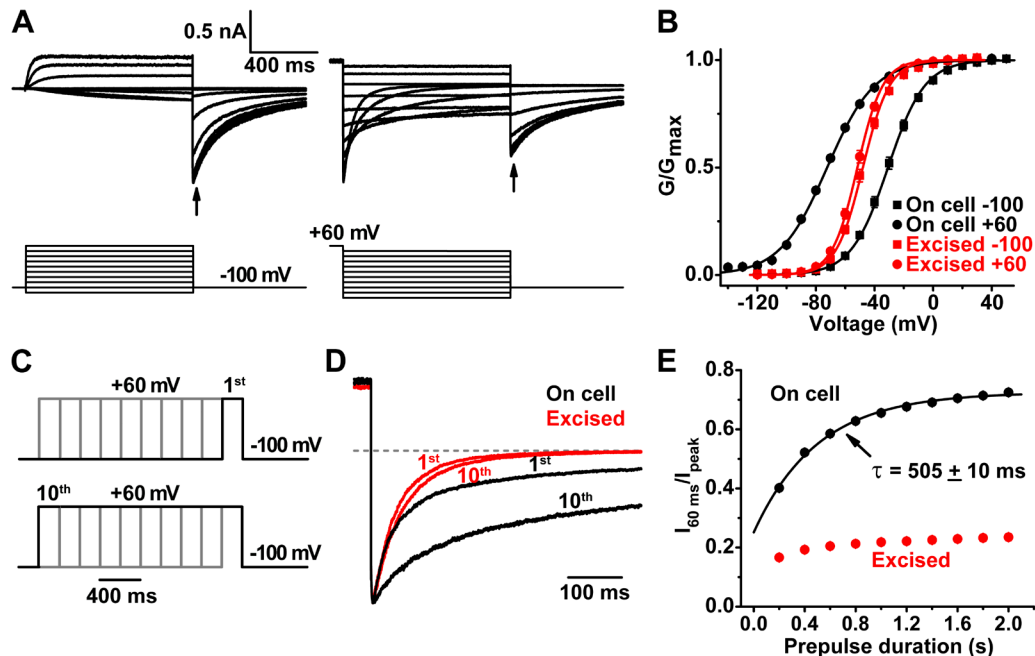

Figure 2. Elk1 has a mode shift to voltage gating that is lost upon patch excision. (A) Elk1 currents are shown for a series of 1-s voltage steps from a holding potential of -100 mV (left) or after a 1-s step to 60 mV to elicit mode shift (right). G-V data were taken from isochronal tail currents at -100 mV (arrows). (B) G-V plots for -100-mV hold (squares) and 60-mV prepulses (circles) in the on-cell (black; $n = 18$) and excised (red; $n = 19$) configurations. Curves are single Boltzmann fits; mode shifts (ΔV_{50} between 60-mV prepulse and -100-mV hold) are reported in Table 2. (C) Voltage protocol for measuring the time course of mode shift. A series of 10 60-mV voltage steps increasing in duration from 200 ms to 2 s were given to activate channels and induce mode shift as estimated by time course of tail currents recorded at -100 mV after the steps. Top and bottom panels depict the 1st and 10th sweeps, respectively. (D) Example tail current traces recorded on cell or excised with voltage protocols shown in C. Only the first and last sweeps are shown for clarity, and data were normalized for display; the dotted line shows the zero current level. (E) Tail current time course measured as fractional amplitude remaining at 60 ms plotted as a function of 60-mV prepulse length ($n = 34$ on cell and 39 excised). The curve for on-cell data are a single-exponential fit with a time constant of 505 ms. All data points show mean $\pm$ SEM.

Elk1 voltage gating has a robust VSD mode shift that is lost upon patch excision

In Erg1, slow deactivation is caused by time-dependent mode shift of the activated voltage sensor (Piper et al., 2003; Tan et al., 2012; Goodchild et al., 2015); the mode-shifted VSD returns to the resting state in a more hyperpolarized voltage range than the original transition from resting to activated. Mode shift is believed to be caused by a relaxation of the VSD into a more stable activated conformation subsequent to its initial activation (Villalba-Galea et al., 2008). We examined mode shift in Elk1 to determine if it could explain the slow

component of deactivation on cell, which is lost upon patch excision. Fig. 2 A shows families of on-cell Elk1 currents recorded in response to voltage steps from -120 to 60 mV from a holding potential of -100 mV (our standard G-V measurement) or with a 1-s prepulse to 60 mV to induce mode shift. The G-V V_{50} measured from isochronal tail currents recorded at -100 mV shifted from -30.8 ± 1.5 mV to -72.3 ± 1.0 mV when we introduced the prepulse to 60 mV (Fig. 2 B). This mode shift reduced from -41.6 ± 1.0 mV to -3.7 ± 0.7 mV after patch excision (Fig. 2 B). The magnitude of the slow component in Elk1 tail currents recorded at -100 mV
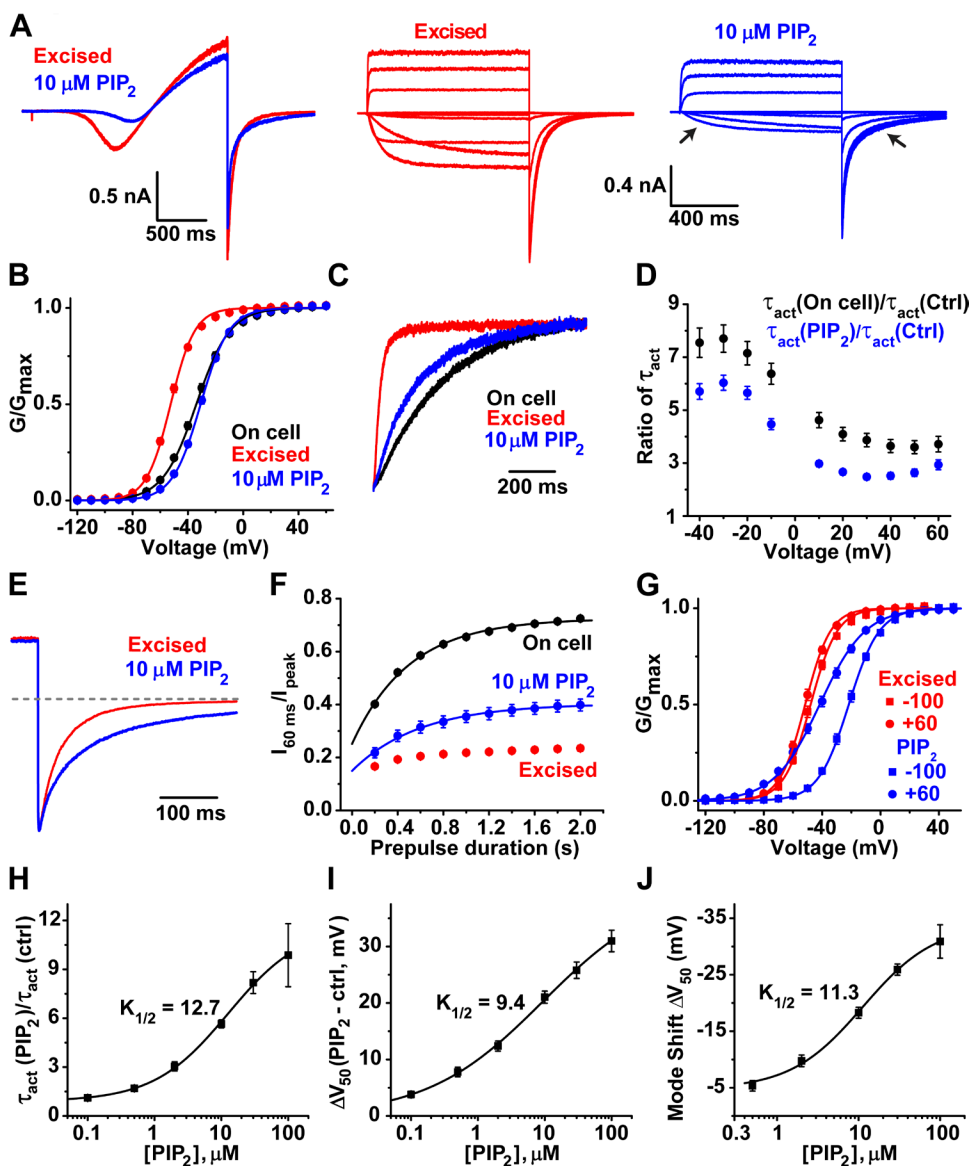

Figure 3. DiC8-PIP$_2$ slows activation and enhances mode shift in Elk1 in excised patches. (A; left) Currents recorded in response to a 2-s voltage ramp (-120 to 80 mV; -100-mV holding potential) before and after the application of 10 µM PIP$_2$. (Middle and right) Currents recorded in response to a series of 1-s voltage steps (-120 to 60 mV in 20-mV increments; -100-mV holding potential) before and after the application of 10 µM PIP$_2$, respectively. Arrows point to slowed activation to deactivation in the PIP$_2$ traces. (B) The application of 10 µM PIP$_2$ shifts Elk1 G-V in the depolarized direction ($n = 37$). On-cell and excised data are the same as in Fig. 1 D. Curves are single Boltzmann fits, and V_{50} and s are reported in Table 1. (C) Normalized current traces from an Elk1 patch comparing the activation rate at -20 mV on cell, excised, and with 10 µM PIP$_2$. Traces were reversed in polarity for display. (D) Change in activation rate upon patch excision and patch application of 10 µM PIP$_2$ at various voltages expressed as τ_{act}(on cell)/τ_{act}(ctrl) and τ_{act}(PIP$_2$)/τ_{act}(ctrl) ($n = 33$ and 18, respectively). (E) Normalized tail currents recorded at -100 mV after 2-s prepulse to 60 mV before and after the application of 10 µM PIP$_2$ (dotted line, zero current). (F) Fractional tail current remaining 60 ms after repolarization to -100 mV in 10 µM PIP$_2$ ($n = 14$; curve is a single-exponential fit with a time constant of 611 ms)

compared with excised and on cell from Fig. 2 E. (G) G-V curves determined from isochronal tail currents at -100 mV after 1-s steps to the indicated voltages for excised controls (red; $n = 19$) and 10 µM PIP$_2$ (blue; $n = 18$) from a holding potential of -100 mV (squares) or with a 1-s prepulse to 60 mV (circles). Mode shift values in millivolts are reported in Table 2. (H–J) Dose–response relationships for PIP$_2$ as measured by $\tau_{act\text{-}PIP2}/\tau_{act\text{-}ctrl}$ at -20 mV (H; $n=5$–20), V_{50} shift (I; $n=14$–26), and G-V mode shift size (J; ΔV_{50}, -100-mV hold vs. 60-mV prepulse; $n = 4$–10). Curves show fits with the Hill equation, and half-maximal concentrations ($K_{1/2}$) are indicated. All data are expressed as mean ± SEM.

on cell (but not excised) was highly sensitive to depolarizing step length (Fig. 2, C–E). We estimated the time course of mode shift at 60 mV by plotting the increase in tail current remaining 60 ms after repolarization to −100 mV (Fig. 2 E). An exponential fit of the data yielded a time constant of 505 ± 10 ms ($n = 34$).

PIP$_2$ slows activation of Elk1 in excised patches and partially restores mode shift

We applied PIP$_2$ to excised patches to determine if the gating changes we observed in Elk1 upon patch excision could be explained by loss of PIP$_2$. We used the diC8 analogue of PIP$_2$ for all experiments because of its enhanced solubility relative to native PIP$_2$. Fig. 3 A shows ramp and step currents from an excised patch before and after the application of 10 µM diC8-PIP$_2$ (referred to as "PIP$_2$" from here on). 10 µM PIP$_2$ depolarized the G-V curve measured from a −100-mV resting potential by 21.7 ± 1.1 mV; the resulting G-V curve was similar to what we observed on cell (Fig. 3 B). 10 µM PIP$_2$ slowed the activation rate of Elk1 relative to excised control conditions (Fig. 3 C) as measured by the ratio of the time constant of activation in PIP$_2$, τ_{act}(PIP$_2$), to the time

constant of activation in control solution, τ_{act}(Ctrl) (Fig. 3 D). The application of 10 µM PIP$_2$ to excised patches also introduced a slow component into tail currents and significantly increased mode shift by 16.2 mV from -3.7 ± 0.7 mV to -19.9 ± 1.3 mV (Fig. 3, E–G).

We calculated the half-maximal PIP$_2$ concentration (K$_{1/2}$) for effects on τ_{act} at −20 mV, G-V V$_{50}$, and mode shift using Hill-equation fits of data at various PIP$_2$ concentrations (Fig. 3, H–J). The K$_{1/2}$ values calculated by each method were similar: 12.7 ± 2.2 µM for τ_{act}, 9.4 ± 2.7 for G-V V$_{50}$, and 11.3 ± 1.7 µM for mode shift. PIP$_2$ could fully restore the slow activation of Elk1 observed on cell at a concentration just above these K$_{1/2}$ values (between 10 and 30 µM; Fig. 3, D and H). Mode shift was not fully restored to excised patches at the same concentrations (Fig. 3 J), suggesting that PIP$_2$ may not fully account for the large on-cell mode shift. These results show that PIP$_2$ regulates the voltage gating of Elk1 in a bimodal fashion by inhibiting voltage activation while enhancing stabilization of open channels. Furthermore, the K$_{1/2}$ values we determined for the application of diC8 PIP$_2$ to excised patches suggest that Elk1 gating could be sensitive to changes in native PIP$_2$ concentrations.
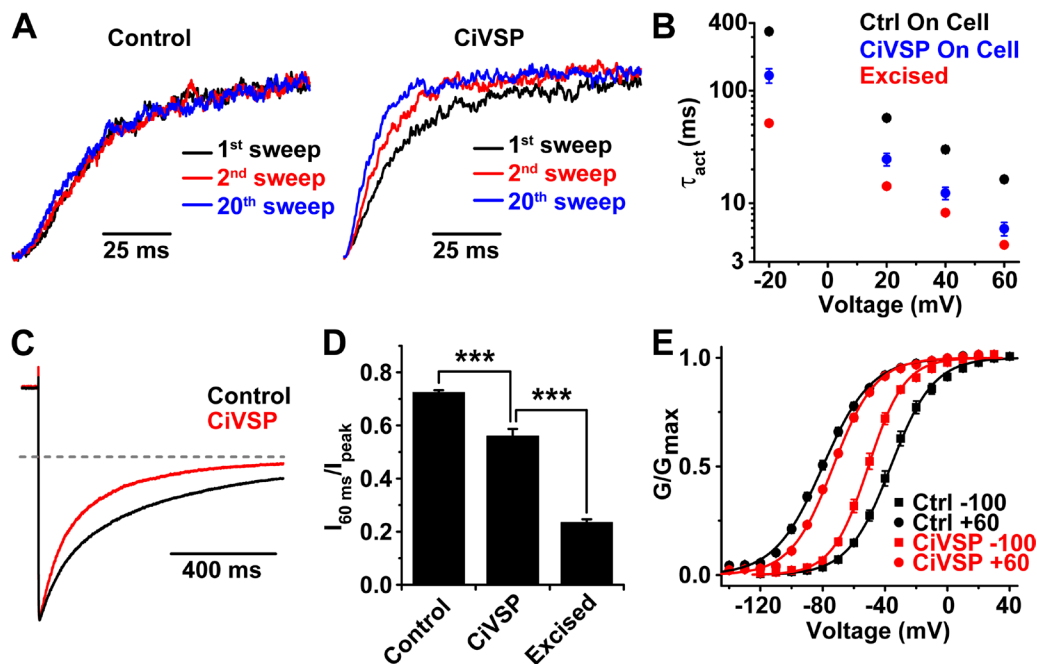

Figure 4. Depletion of native PIP$_2$ with CiVSP alters Elk1 gating kinetics. (A) Normalized Elk1 current traces recorded at 60 mV on cell patches from an Elk1 control and Elk1 + CiVSP. Repeated 2-s steps to 60 mV were delivered at 6-s intervals, and the 1st, 2nd, and 20th sweeps are shown for comparison. (B) Activation time constants at various voltages determined for Elk1 + CiVSP on cell patches ($n = 5$) and compared with Elk1 on cell and excised controls from Fig. 1 F. The on-cell time constant significantly decreased at all voltages measured (P < 0.001; t test) with CiVSP coexpression. (C) Normalized tail current traces at −100 mV after 2-s prepulse to 60 mV. The first sweep is shown for each condition, and the tail shape did not change with further repeated sweeps (dotted line, zero current). (D) Deactivation time course measured as fractional tail current remaining 60 ms after repolarization to −100 mV after a 2-s prepulse to 60 mV ($n = 34$, 16, and 39 for on-cell control, + CiVSP, and excised control, respectively; ***, P < 0.001; t test). (E) On-cell G-V curves for Elk1 controls (black; $n = 5$) and +CiVSP (red; $n = 4$) recorded from the typical −100-mV hold (squares) and with a 1-s 60-mV prepulse (circles). Curves show single Boltzmann fits, and G-V mode shift values (circle V$_{50}$ − square V$_{50}$) are reported in Table 3. All data are reported as mean ± SEM.

Depletion of native PIP_2 with CiVSP modulates Elk1 voltage gating

Although a huge diversity of channels is regulated by PIP_2 as measured by patch excision and direct PIP_2 application to the intracellular face of patches, only a subset of channels appears to be regulated by changes in PIP_2 concentration in intact cells (Hilgemann, 2012; Kruse et al., 2012; Kruse and Hille, 2013). In cases where channel activity requires PIP_2, but is not modulated by physiological changes in PIP_2 concentration, it has been suggested that constitutive PIP_2 binding might be necessary for normal channel function (Hilgemann et al., 2001; Suh and Hille, 2008; Hilgemann, 2012; Kruse et al., 2012; Zhou and Logothetis, 2013). We therefore examined whether depletion of native PIP_2 by the depolarization-activated phosphoinositide 5-phosphatase CiVSP (Murata et al., 2005; Halaszovich et al., 2009) could alter the gating of Elk1 in on-cell patches. Repeated depolarization of whole oocytes expressing CiVSP under two-electrode voltage clamp depletes PIP_2 sufficiently to inhibit PIP_2-dependent KCNQ currents (Li et al., 2015a). Oocytes for patches are often damaged during removal of the vitelline envelope, and we bathed the oocytes in high K^+ intracellular recording solution, so it is reasonable to assume that they were sufficiently depolarized for some basal CiVSP activation and PIP_2 depletion before patch formation. Indeed, activation of Elk1 currents was already fast in most CiVSP-expressing versus control patches during the first depolarizing voltage step applied to the patch. Nevertheless, repeated depolarizing steps to 60 mV further increased the rate of activation in some patches, a change that was never observed in control oocytes (Fig. 4 A). The mean activation time constants for on-cell patches recorded from CiVSP-expressing oocytes in response to increasing voltage steps were significantly smaller than for control oocytes (Fig. 4 B). However, CiVSP coexpression does not speed up activation as much as patch excision (Fig. 4 B), possibly because of incomplete depletion of native PIP_2 during the steps or rapid PIP_2
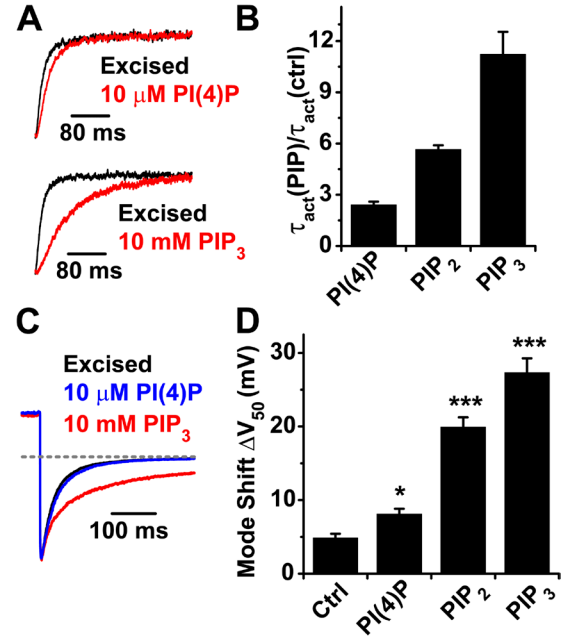

Figure 5. Elk1 modulation by diC8-PI(4)P and diC8-PIP_3. (A) Normalized currents compare Elk1 activation at 20 mV before and after the application of the indicated PIP. (B) Fold changes in activation time constant at −20 mV upon the application of 10 µM of the indicated PIP (n = 9, 18, and 10 for PI(4)P, PIP_2, and PIP_3, respectively). (C) Normalized tail currents recorded at −100 mV after a 2-s prepulse to 60 mV before and after the application of 10 µM PI(4)P and PIP_3 (dotted line, zero current). (D) G-V mode shift induced by 10 µM of the indicated PIPs, measured as in Fig. 2 B. All data show mean ± SEM; n = 32, 9, 18, and 9 for control, PI(4)P, PIP_2, and PIP_3, respectively; *, P < 0.05; ***, P < 0.001; t test.

resynthesis between steps. Similarly, the deactivation time course was significantly faster in CiVSP-expressing oocytes (Fig. 4, C and D), and mode shift was significantly reduced from −41.6 ± 1.9 mV in control oocytes to −22.0 ± 1.4 mV in CiVSP-expressing oocytes (Fig. 4 E). These results suggest that native PIP_2 in oocytes modulates Elk1 the same way as diC8-PIP_2 in excised patches.

TABLE 2

Mode shifts shown as ΔV_{50} in millivolts for G-V curves measured with a 1-s 60-mV prepulse compared to a −100-mV holding potential

Channel	On cell			Excised			10 µM PIP_2		
	Mean	SEM	n[a]	Mean	SEM	n	Mean	SEM	n
WT	−41.6[b]	1.0	18	−3.7	0.7	19	−19.9	1.3	18
Δ2–136	−6.2	1.1	9	−4.4	1.6	7	−1.3	1.9	7
K5Q	−26.7	1.3	11	−3.1	1.2	9	−7.4	1.1	8
R347E	−19.3	1.2	6	−4.1	1.1	6	−3.5	2.4	6
R347C	−40.7	1.7	8	−4.3	2.0	7	−11.3	1.9	6
R475E	−46.5	1.5	8	−5.7	0.4	8	−19.6	1.8	8
R479E	−21.8	1.2	16	−7.0	1.3	7	−9.5	1.0	5
R479Q	−26.9	2.3	5	−2.9	1.1	5	−8.0	2.0	5

[a]n, number of measurements.
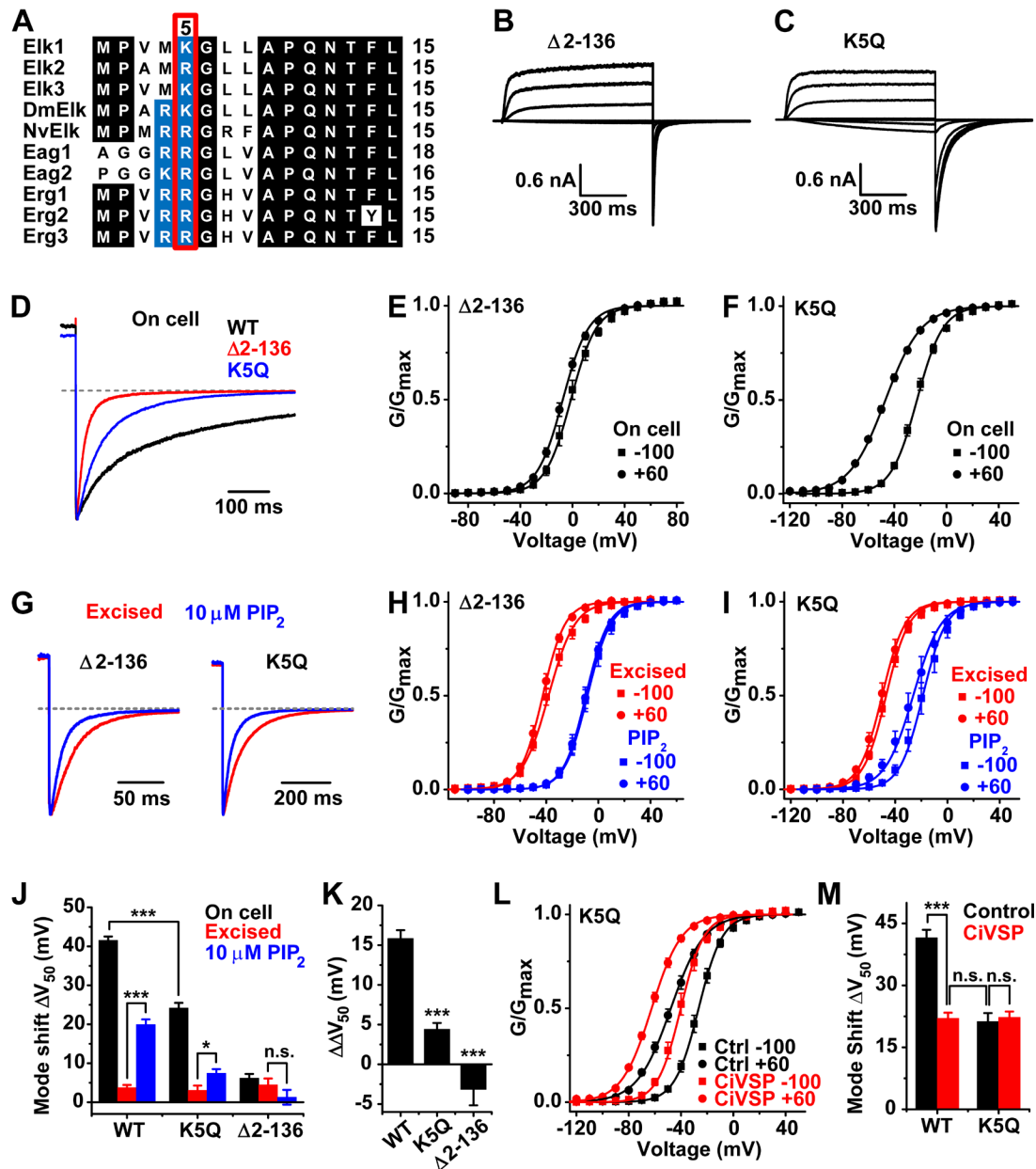[b]ΔV_{50}, mV.

Figure 6. Role of the Elk1 N-terminal eag domain in mode shift. (A) Sequence alignment of the first 15 amino acids of the Cap domain for all human EAG family channels and fly (Dm) and *Nematostella* (Nv; sea anemone) Elk orthologues. Basic residues are shaded in blue, and other residues conserved in at least eight sequences are shaded in black. A universally conserved basic residue (K5 in Elk1) is highlighted with the red box. (B and C) On-cell current traces recorded in response to 1-s steps (-120 to 60 mV in 20-mV increments; -100-mV holding potential) for Elk1 $\Delta 2$–136 and K5Q. (D) Normalized on-cell tail currents recorded at -100 mV after 1-s prepulse to 60 mV for $\Delta 2$–136 and K5Q compared with WT (dotted line, zero current). (E and F) On-cell G-V curves recorded from a -100-mV hold (squares) or with a 1-s 60-mV prepulse (circles) for $\Delta 2$–136 and K5Q. (G) Normalized $\Delta 2$–136 and K5Q tail currents recorded at -100 mV after a 1-s prepulse to 60 mV from excised patches before and after the application of 10 µM PIP_2. (H and I) G-V curves for $\Delta 2$–136 and K5Q determined from isochronal tail currents at -100 mV after 1-s steps to the indicated voltages for excised controls (red) and 10 µM PIP_2 (blue) from a holding potential of -100 mV (squares) or with a 1-s prepulse to 60 mV (circles). (J) Mode shift values for $\Delta 2$–136 and K5Q compared with WT (*, $P < 0.05$; ***, $P < 0.001$; t test), on cell (black), excised (red), and plus 10 µM PIP_2 (blue). (K) PIP_2-dependent mode shift ($\Delta \Delta V_{50}$, 10 µM PIP_2-exised control) for WT, K5Q, and $\Delta 2$–136 (***, $P < 0.001$ vs. WT; t test). (L) On-cell G-V curves for K5Q controls and +CiVSP recorded from a -100-mV hold (squares) or with a 1-s 60-mV prepulse (circles). (M) Mode shift measured on cell with or without CiVSP coexpression for K5Q compared with WT (***, $P < 0.001$; t test). All data are mean ± SEM; sample numbers are provided in Tables 1–3, and curves in G-V panels show single Boltzmann fits. GenBank accession numbers for the full sequences aligned in A are: Elk1, NM_144633; Elk2, NM_012284; Elk3, NM_012285; Eag1, NM_172362; Eag2, NM_139318; Erg1, NM_000238; Erg2, NM_030779; Erg3, NM_033272; DmElk, NM_057661; NvElk, KM_052387.
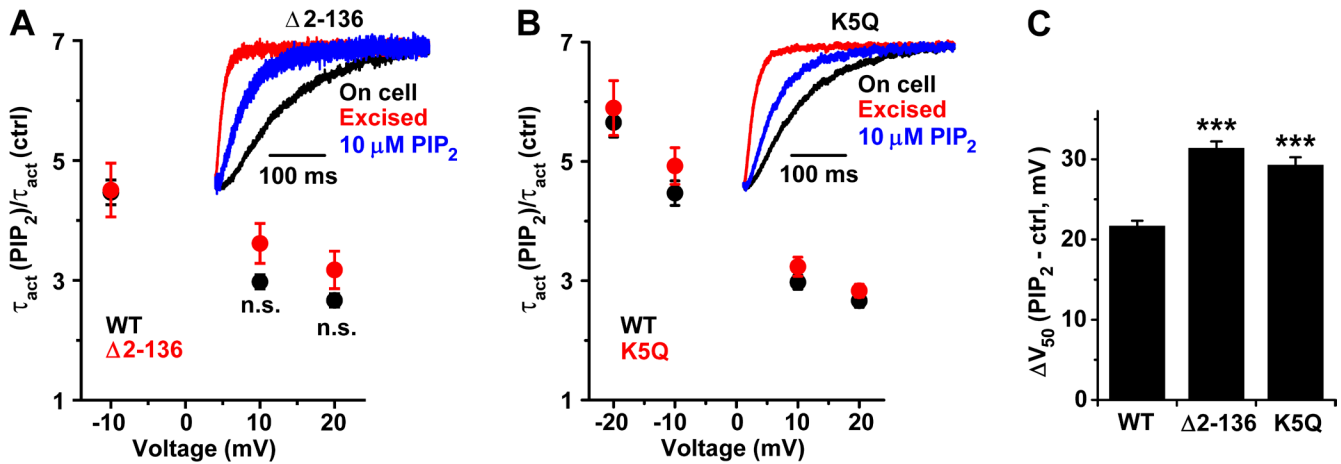
Figure 7. PIP$_2$ inhibits activation in Elk1 $\Delta 2$–136 and K5Q mutants. (A) τ_{act}(10 µM PIP$_2$)/τ_{act}(Ctrl) at various voltages compared for WT ($n = 18$) and $\Delta 2$–136 ($n = 9$). Accurate measurement of the $\Delta 2$-136 activation time constant below -10 mV was not possible in 1-s steps because of the depolarized G-V. The inset compares normalized currents for a $\Delta 2$-136 patch at 10 mV on cell, excised, and in the presence of 10 µM PIP$_2$. (B) Repeat of A for K5Q ($n = 8$). (C) ΔV_{50} induced by 10 µM PIP$_2$ in excised patches for WT, $\Delta 2$–136, and K5Q ($n = 37$, 14, and 8, respectively; ***, P < 0.001 vs. WT; t test).

PIP$_2$ and PIP$_3$ regulate Elk1

We tested the ability of the diC8 analogues of two other plasma membrane phosphoinositides, phosphatidylinositol 4-phosphate (PI(4)P) and phosphatidylinositol (3,4,5)-trisphosphate (PIP$_3$), to modulate the voltage gating of Elk1. PI(4)P is the precursor for PIP$_2$ synthesis and is the major metabolite produced from PIP$_2$ by CiVSP (Halaszovich et al., 2009). PIP$_3$ is typically >100-fold less abundant than PIP$_2$ in cells (Vanhaesebroeck et al., 2001) but strongly modulates CNG channel gating (Zhainazarov et al., 2004; Brady et al., 2006; Bright et al., 2007). Elk1 activation rates with the application of 10 µM of each diC8 phosphoinositide are compared in Fig. 5 (A and B). PIP$_3$ slowed activation significantly more than PIP$_2$, whereas PI(4)P had only a small effect on activation at 10 µM. The same rank order of effect (PIP$_3$ > PIP$_2$ > PI(4)P) was observed at the applied 10-µM concentration for mode shift (Fig. 5, C and D). The small effects observed for PI(4)P relative to PIP$_2$ are consistent with the ability of the phosphoinositide 5-phosphatase CiVSP to enhance activation rate and reduce mode shift in Elk1. These data suggest that phosphoinositide regulation of Elk1 could occur through either PIP$_2$ or PIP$_3$, although we did not fully explore the affinity and efficacy of PIP$_3$ for this study. We instead focused on PIP$_2$ modulation for this study to facilitate comparison to the broad literature on PIP$_2$ regulation of channels.

The role of the eag domain in mode shift

We next examined which domains of Elk1 might be responsible for the PIP$_2$ dependence of voltage gating. Because the eag domain and conserved basic residues at the N terminus of the Cap support mode shift in hErg1 (Tan et al., 2012), we deleted the entire eag domain of Elk1 ($\Delta 2$–136), or alternatively neutralized a single conserved basic residue in the N-terminal Cap (K5Q), to test the role of the Elk1 eag domain in open-state stabilization. K5 aligns with a Cap residue (R5) that plays a role in mode shift in Erg1 (Fig. 6 A). Elk1 $\Delta 2$–136 and K5Q currents recorded on cell in response to voltage steps are shown in Fig. 6 (B and C), and the time course of on-cell tail currents recorded after a 1-s 60-mV pulse is compared with WT in Fig. 6 D. Elk1 $\Delta 2$–136 tail currents were extremely rapid on cell compared with WT, whereas K5Q tail currents were intermediate between

TABLE 3
Mode shifts on cell ± CiVSP (ΔV_{50} in G-V curves measured with a 1-s 60-mV prepulse or from a -100-mV holding potential)

Channel	Control			+CiVSP		
	Mean	SEM	n[a]	Mean	SEM	n
WT	-41.6[b]	1.9	5	-22.0	1.4	4
K5Q	-21.6	2.0	8	-22.3	1.4	12
R347E	-18.6	1.3	5	-15.5	0.9	5
R479E	-14.5	1.5	5	-10.0	3.0	7

[a]n, number of measurements.
[b]ΔV_{50}, mV.

the two. Mode shift on cell was almost completely eliminated in Elk1 Δ2–136 (-6.2 ± 3.1 mV; $n = 9$) and reduced significantly to -26.7 ± 1.7 mV ($n = 11$; $P < 0.0001$; t test) for Elk1 K5Q (Fig. 6, E and F, and Table 2). Neither mutant exhibited mode shift after excision; 10 µM PIP_2 actually accelerated deactivation and introduced a small but significant increase in mode shift for K5Q but not Δ2–136 (Fig. 6, G–J, and Table 2). However, the increase in mode shift in excised patches caused by 10 µM PIP_2 relative to control solution ($\Delta\Delta V_{50}$) was significantly reduced in both K5Q and Δ2–136 versus WT (Fig. 6 K). The accelerated deactivation we observed for both mutants in 10 µM PIP_2 (Fig. 6 G) is likely a consequence of the large depolarized G-V shifts in the presence of PIP_2 (Fig. 6, H and I), and we did not study it further. Finally, the on-cell mode shift of Elk1 K5Q was

not reduced by coexpression with CiVSP (Fig. 6, L and M, and Table 3) and was identical in magnitude to the mode shift remaining for Elk1 WT after depletion of PIP_2 by CiVSP (-21.3 ± 2.0 mV vs. -22.0 ± 1.4 mV; $P = 0.76$; $n = 8$ and 4, respectively). These results indicate that the eag domain is required for open-state stabilization and the accompanying mode shift in Elk1, and that K5 in the Cap increases the ability of PIP_2 to promote stabilization and mode shift.

We reasoned that the ability of PIP_2 to inhibit voltage activation in Elk1 K5Q and Δ2–136 mutants might be intact because of the large rightward shift of the G-V after 10 µM PIP_2 application to excised patches (Fig. 6, H and I) and the leftward G-V shift observed for K5Q in the presence of CiVSP (Fig. 6 L). The activation rates of Elk1 Δ2–136 and K5Q were indeed slowed by PIP_2 (Fig. 7, A and B), indicating that other regions of the Elk1 channel must mediate inhibitory effects of PIP_2. The fold changes of τ_{act} caused by 10 µM PIP_2 relative to excised controls were similar for Δ2–136, K5Q, and WT (Fig. 7, A and B). However, the rightward G-V shift caused by 10 µM PIP_2 was significantly increased for both mutants (Fig. 7 C). PIP_2-dependent G-V shifts reflect a composite of PIP_2-dependent inhibition of activation counterbalanced by mode shift. We hypothesize that the depolarizing G-V shifts are bigger in K5Q and Δ2–136 because the counterbalancing effect of mode shift is significantly reduced.

Basic residues in the S4–S5 linker and post-S6 are required for PIP_2-dependent inhibition of Elk1

Basic residues at the cytoplasmic interface of the VSD and S6 activation gate have been implicated in PIP_2-dependent inhibition of Shaker channel gating (Rodriguez-Menchaca et al., 2012a) and PIP_2-dependent coupling of VSD activation to pore opening in KCNQ channels (Zaydman et al., 2013). We therefore tested whether basic residues in the S4–S5 linker (R347) and post-S6 (R475 and R479) of Elk1 (Fig. 8, A and B) were required for PIP_2-dependent modulation of Elk1 gating using charge-reversal and neutralization substitutions. R347E was functional (Fig. 9 A) but exhibited significantly smaller changes in activation rate relative to WT upon the application of 10 µM PIP_2 (Fig. 9, A and B). Furthermore, deactivation was more rapid on cell in R347E, and PIP_2 did not introduce a slow component in excised patches (Fig. 9 C). In contrast, PIP_2 strongly inhibited activation of R347C and introduced a small slow component into the tail (Fig. 9, D–F). On-cell mode shift was significantly reduced in in R347E, and PIP_2 did not significantly increase mode shift in excised patches (Fig. 9 G and Table 2). We hypothesize that R347E retains the ability to mode shift but lacks PIP_2-dependent enhancement of mode shift. In contrast, R347C had normal mode shift on cell but significantly reduced PIP_2-dependent enhancement of mode shift in excised

A

```
Elk1    L L Q K L D R Y S Q H S T I V L   356
Elk2    L L P R L D R Y S Q Y S A V V L   359
Elk3    L L Q K L E R Y S Q C S A V V L   361
DmElk   L L Q K I D R Y S Q H T A M I L   399
NvElk   V V R K L H R Y S E Y S T V L L   355
Eag1    V A R K L D H Y I E Y G A A V L   351
Eag2    V A R K L D H Y L E Y G A A V L   348
Erg1    V A R K L D R Y S E Y G A A V L   549
Erg2    V A R K L D R Y S E Y G A A V L   400
Erg3    V A R K L D R Y S E Y G A A V L   551
Kv1.2   G Q T L K A S M R E L G L L I F   333
KCNQ1   G S V V F I H R Q E L I T T L Y   267
                     S45L              S5
```

B

```
Elk1    G N V T A I I Q R M Y S R W S L   482
Elk2    G N V T A I I Q R M Y A R R F L   513
Elk3    G N V T A I I Q R M Y S R R S L   487
DmElk   G N V T A I I Q R M Y S R R S L   517
NvElk   G N V T A I I Q K L Y A N R V R   478
Eag1    G N V T T I F Q Q M Y A N T N R   484
Eag2    G N V T T I F Q Q M Y A N T N R   480
Erg1    G N V S A I I Q R L Y S G T A R   672
Erg2    G N V S A I I Q R L Y S G T A R   524
Erg3    G N V S A I I Q R L Y S G T A R   675
Kv1.2   P V I V S N F N Y F Y H R E T E   422
KCNQ1   G I L G S G F A L K V Q Q K Q R   360
                S6              Post-S6
```
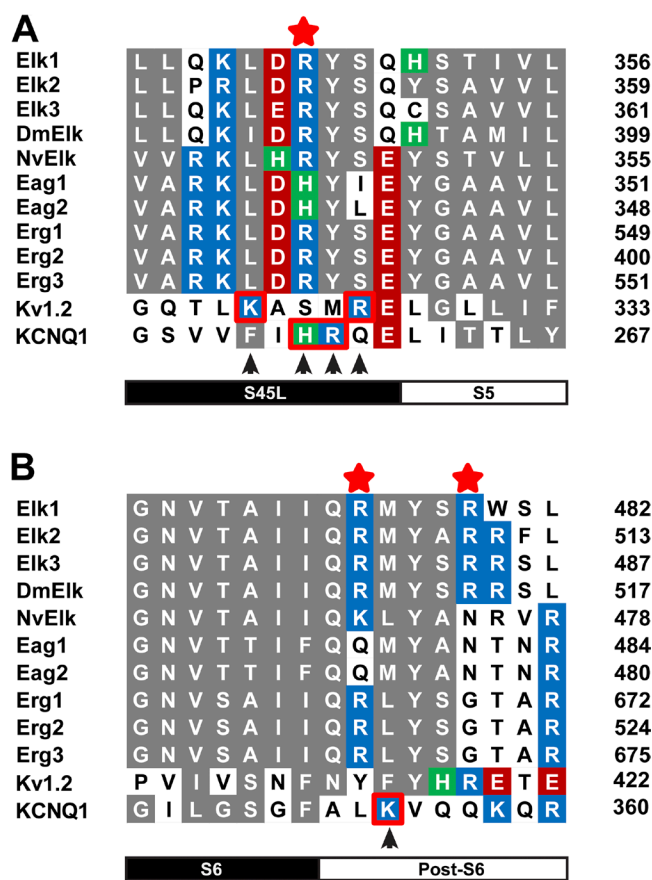
Figure 8. Sequence alignments of the S4–S5 linker (A) and post-S6 (B) for all human EAG family channels, *Drosophila* and *Nematostella* Elk, and human Kv1.2 and KCNQ1. Basic residues Lys and Arg are shaded blue, and His is shaded green. Acidic residues are shaded red, and other positions with general conservation are shaded gray. Elk1 R347, R475, and R479 are marked with red stars; Kv1.2 and KCNQ1 residues required for PIP_2 modulation are outlined in red. Domain boundaries are indicated below the alignments, and sequence positions are indicated at the right margin. GenBank sequence accession numbers for EAG family channels are given in the legend to Fig. 6, and are NM_004974 and NM_000218 for Kv1.2 and KCNQ1, respectively.

patches ($\Delta\Delta V_{50}$, -7.3 ± 1.2 mV [$n = 6$] vs. -15.8 ± 1.1 mV [$n = 18$] for WT; P < 0.001). Patch excision had little effect on the G-V of R347E, but 10 µM PIP$_2$ caused a 20.6 $\pm$ 3.6–mV shift in V$_{50}$ (Fig. 9 H and Table 1). This is similar to what we observed for WT but less than what we observed for K5Q, which has normal PIP$_2$-dependent inhibition of activation but (like R347E) lacks the counterbalance of PIP$_2$-dependent enhancement of mode shift. This reduction in the PIP$_2$-dependent depolarizing G-V shift relative to K5Q supports our observation that PIP$_2$ has a reduced ability to inhibit activation in R347E. The PIP$_2$-dependent depolarizing G-V shift was similar in R347C (22.9 ± 2.5 mV; Fig. 9 I) but was likely constrained by residual PIP$_2$-dependent mode shift (Fig. 9 G).

Charge-reversal mutations at R475 (R457E) and R479 (R479E) had differential effects on PIP$_2$-dependent inhibition of voltage activation (Fig. 10, A–C). PIP$_2$ slowed voltage activation of R475E in a similar fashion to WT, whereas the effects of PIP$_2$ on activation were significantly reduced in R479E, as quantified by the fold change in the activation rate induced by 10 µM PIP$_2$. R475E also had a large mode shift on cell and normal PIP$_2$-dependent enhancement of mode shift when excised (Fig. 10 D and Table 2). In contrast, on-cell mode shift was significantly reduced for R479E, and PIP$_2$ did not recover mode shift in excised patches (Fig. 10 D and Table 2). The R475E G-V shifts upon excision and 10 µM PIP$_2$ application were unexpectedly less than we observed for
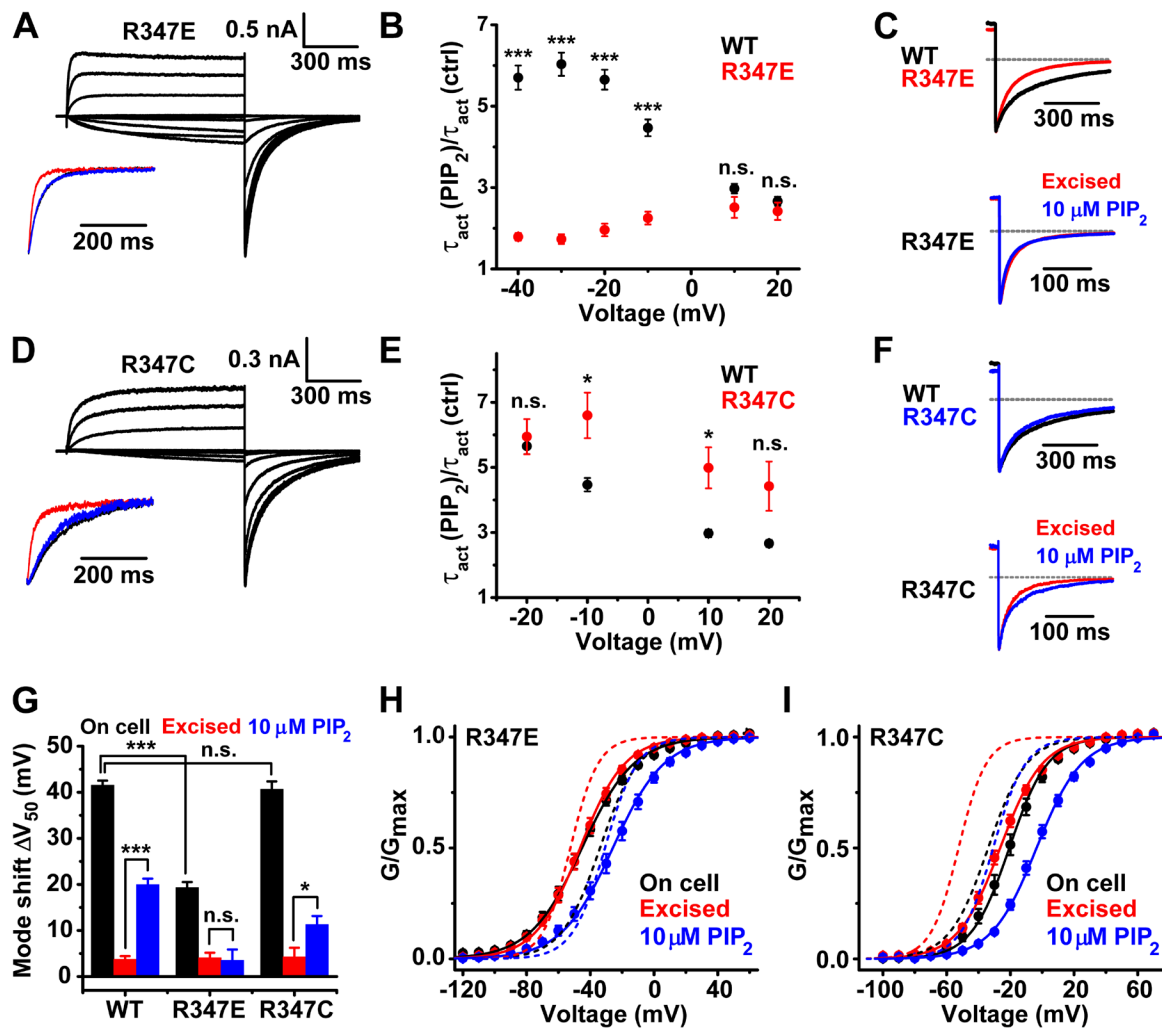

Figure 9. Effect of R347 mutations on the PIP$_2$ modulation of Elk1. (A) R347E on cell currents recorded in response to 1-s voltage steps (-120 to 60 mV in 20-mV increments) from a holding potential of -100 mV. Insets show normalized currents at 20 mV from a patch on cell (black), excised (red), and plus 10 µM PIP$_2$ (blue). (B) $\tau_{act}(10$ µM PIP$_2)/\tau_{act}$(Ctrl) at various voltages for R347E ($n = 9$) and WT ($n = 18$). ***, P < 0.001; t test. (C) Normalized tail currents recorded at -100 mV after a 1-s prepulse to 60 mV, comparing R347E to WT on cell (top) and R347E excised before and after 10 µM PIP$_2$ application (bottom). (D–F) Repeat of A–C for R347C ($n = 8$); *, P < 0.05; t test. (G) G-V mode shift measured as in Fig. 2 (A and B) for R347 mutants compared with WT on cell, excised, and plus 10 µM PIP$_2$ (n reported in Table 2; *, P < 0.05; ***, P < 0.001; t test). (H and I) G-V curves for R347E and R347C on cell (black), excised (red), and plus 10 µM PIP$_2$ (blue) recorded from a -100-mV holding potential. V$_{50}$, s, and n numbers are reported for each plot in Table 1, and corresponding WT G-V curves are shown with dotted lines for comparison. All data are presented as mean $\pm$ SEM.

WT (Fig. 10 E and Table 1), but we did not explore this further because PIP$_2$-dependent mode shift and inhibition of activation were normal when assayed individually. R479E had a depolarizing shift in G-V upon patch excision, and 10 µM PIP$_2$ did not depolarize the G-V further (Fig. 10 F and Table 1). This phenotype is consistent with a large reduction in bimodal PIP$_2$ regulation. Neutralization of R479 (R479Q) showed a parallel but less severe phenotype to R479E (Fig. 10, G–I, and Tables 1 and 2). Inhibition of activation in R479Q was significantly reduced relative to WT. R479Q on-cell mode shift was also significantly reduced, but a small

amount of PIP$_2$ enhancement of mode shift remained. These data argue that R479 (but not R475) has a strong influence on PIP$_2$-dependent modulation of voltage gating in Elk1.

We further explored the roles of R347 and R479 in PIP$_2$-dependent gating by examining the effect of native PIP$_2$ depletion by CiVSP on these mutants. The activation rate of R347E was consistently faster at a given voltage in the presence of CiVSP, but the changes were small and only significant at −40 mV (Fig. 11, A and B). CiVSP did not alter the R347E G-V curves or significantly reduce on-cell mode shift (Fig. 11, C and D). R479E
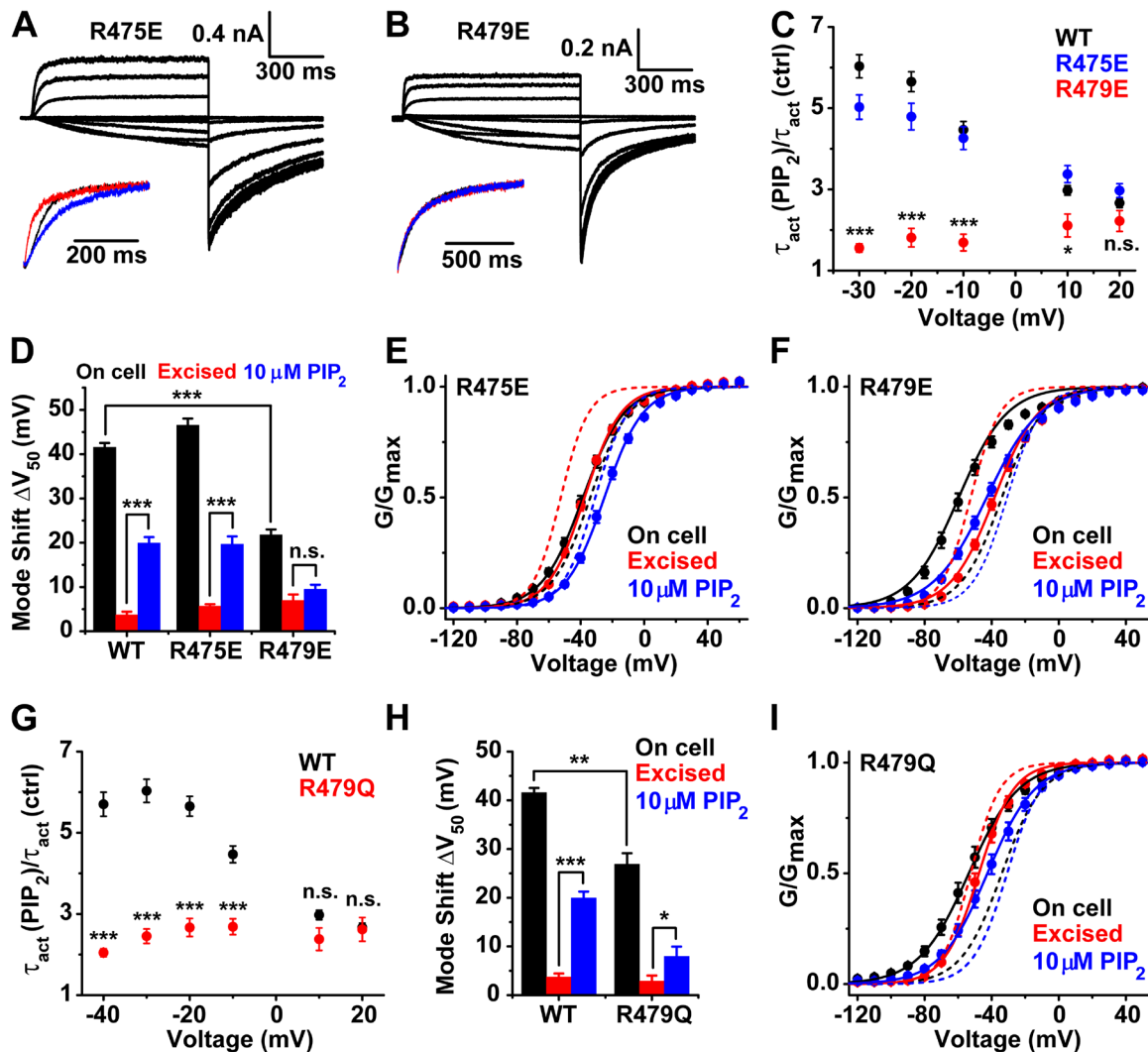

Figure 10. Effect of R475 and R479 mutations on the PIP$_2$ modulation of Elk1. (A and B) R475E and R479E current traces recorded in response to 1-s voltage steps (−120 to 60 mV in 20-mV increments; −100-mV holding potential) in the on-cell configuration. (Insets) Normalized current traces at 20 mV for R475E and at −20 mV for R479E (reversed in polarity for display) comparing on cell (black), excised (red), and plus 10 µM PIP$_2$ (blue). (C) τ_{act}(10 µM PIP$_2$)/τ_{act}(Ctrl) at various voltages compared for R475E ($n = 20$), R479E ($n = 10$), and WT ($n = 18$). R479E differed from WT as indicated: *, P < 0.05, or ***, P < 0.001. (D) G-V mode shift determined with protocols shown in Fig. 2 A for the indicated mutants and conditions (n numbers in Table 2; ***, P < 0.001; t test). (E and F) G-V curves for R475E and R479E on cell (black), excised (red), or plus 10 µM PIP$_2$ (blue; dotted lines, corresponding WT). V$_{50}$, s, and n numbers are reported in Table 1. (G–I) Repeat of C–E for R479Q. R479Q, $n = 5$ in G; H and I, sample numbers are reported in Tables 1 and 2, with ΔV$_{50}$ and Boltzmann parameters, respectively (*, P < 0.05; **, P < 0.01; ***, P < 0.001 vs. WT; t test). All data are mean ± SEM, and curves in E, F, and I show single Boltzmann fits.

had essentially the same phenotype in the presence of CiVSP, except no significant changes in activation rate were observed and there was a small right shift in the G-V curves (Fig. 11, E–G). R479E mode shift on cell was slightly smaller than what we observed in previous experiments, but it was not further reduced by CiVSP (Fig. 11 H). The relative insensitivity of R347E and R479E to CiVSP further supports the conclusion that these mutants have reduced bimodal PIP$_2$ modulation.

DISCUSSION

Elk1 is the first example of an EAG family channel that displays bimodal regulation of voltage gating by PIP$_2$. This regulation is in part mediated by two basic residues in the S4–S5 linker (R347) and post-S6 region (R479). The residues are required for both PIP$_2$-dependent inhibition of voltage gating and PIP$_2$-dependent stabilization of open channels. One important open question regarding the bimodal regulation of voltage-gated channels by PIP$_2$ has been whether the sites for inhibition and enhancement are spatially separate or overlapping (Zhou and Logothetis, 2013). Our functional data suggest that the sites could overlap in Elk1. Because the S4–S5 linker and cytoplasmic edge of S6 are the site of coupling between the VSD and activation gate (Chen et al., 2001; Tristani-Firouzi et al., 2002; Long et al., 2005a,b), these basic residues could lie in close proximity and conceivably have direct electrostatic interactions

with PIP$_2$, as has been suggested for similarly placed residues in KCNQ channels (Zaydman et al., 2013; Zaydman and Cui, 2014). Direct S4–S5 linker and post-S6 (TRP-box) interactions with PIP$_2$ mediated by basic residues have also been proposed for Kv1.2 (Rodriguez-Menchaca et al., 2012a) and TRP channels (Rohács et al., 2005; Poblete et al., 2015), respectively. This mechanism is appealing because PIP$_2$–protein interactions are typically mediated by direct binding to basic residues (Suh and Hille, 2008). However, our data do not differentiate between direct binding and allosteric interaction between the S4–S5 linker/post-S6 and PIP$_2$ bound at an alternate site(s). Basic residues in the C-linker have been shown previously to be involved in PIP$_2$-dependent inhibition of HCN channels (Flynn and Zagotta, 2011), which may be equivalent to the open-state stabilization we observed for Elk1 in our study. The Elk1 C-linker has similarly positioned basic residues, but we did not examine their role in PIP$_2$-dependent modulation in this study.

Suh and Hille (2008) proposed two alternate models of how PIP$_2$ can interact with ion channels: (1) a tight pocket with high affinity and specificity for PIP$_2$, or (2) a more general electrostatic interaction with lower affinity and less selectivity between phosphoinositides. Our Elk1 data are supportive of a binding site with the latter characteristics. The affinity for PIP$_2$ (K$_{1/2}$ of roughly 10 µM) is relatively low, and PIP$_3$ also had a strong bimodal effect on gating. The main requirement for
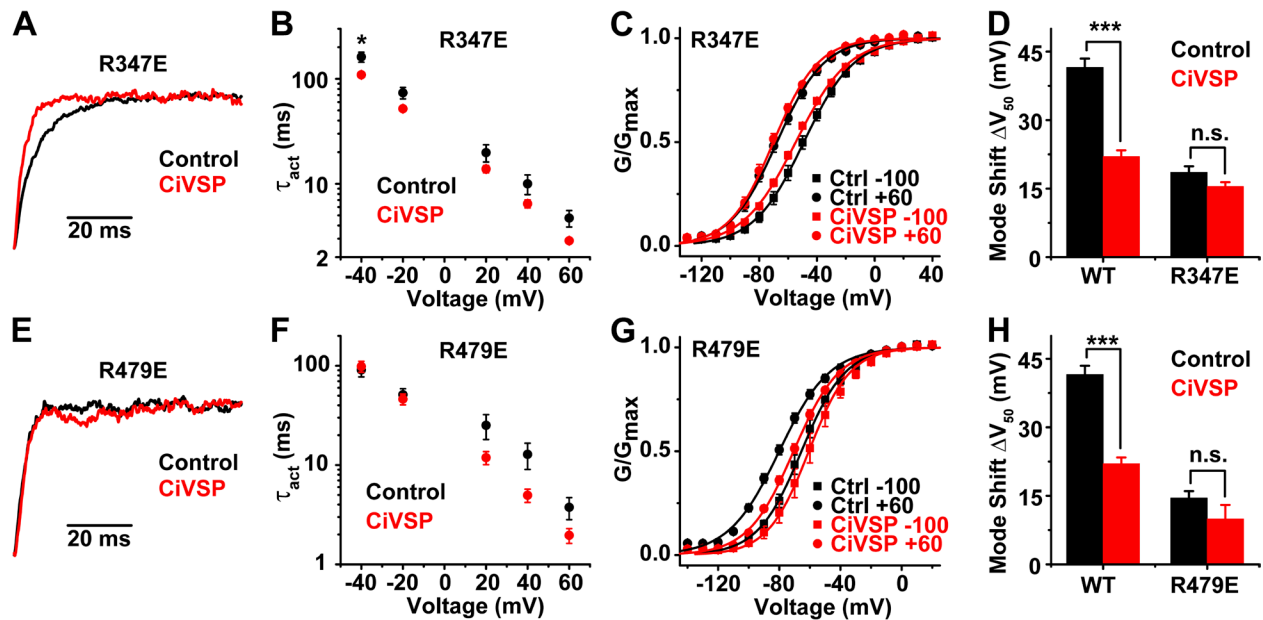

Figure 11. Effects of depletion of native PIP$_2$ with CiVSP on R347E and R479E. (A) Normalized currents recorded at 60 mV for R347E in the presence or absence of CiVSP. (B) Activation time constants on cell with ($n = 6$) or without ($n = 5$) CiVSP. (C) On-cell G-V curves for R347E controls (black; $n = 5$) and +CiVSP (red; $n = 5$) recorded from the typical −100-mV hold (squares) and with a 1-s 60-mV prepulse (circles). Curves show single Boltzmann fits, and mode shift values are reported in Table 3 and plotted in D. (D) R347E mode shift measured on cell with or without CiVSP coexpression compared with WT. (E–H) Repeat of A–D for R479E ($n = 3$–5 for F and 5–7 for G and H). All data are mean ± SEM (*, P < 0.05; ***, P < 0.001; t test).

strong modulation appears to be the presence of multiple phosphate groups on the inositol ring, as PI(4)P has much less effect on gating. A more general association between PIP_2 and the cytoplasmic gating machinery of voltage-gated channels is also suggested by sequence conservation of the S4–S5 linker and post-S6. For instance, basic residues within these regions are required for PIP_2-dependent modulation of gating in Elk1, KCNQ1, and Kv1.2, but the precise side chain, position, and pattern of basic residues are variable (Fig. 8, A and B). We suggest that PIP_2 might be able to be accommodated at the activation gates of most voltage-gated channels, but its effects on gating will vary based on the precise contacts made. In this manner, PIP_2 regulation could be conserved across the voltage-gated superfamily yet plastic through evolutionary time; various aspects of PIP_2 modulation might come and go rapidly as the gating machinery sequence evolves. For instance, evidence so far suggests that KCNQ channels, which strictly require PIP_2 for activation, probably evolved from the Shaker family sometime after the evolution of the first nervous systems (Li et al., 2015a). Shaker family channels vary with respect to PIP_2 modulation (Hilgemann et al., 2001; Kruse et al., 2012; Rodriguez-Menchaca et al., 2012a; Kruse and Hille, 2013), but most do not require PIP_2. Shakers from cnidarians are stable in excised patches (Jegla et al., 2012), so this lack of a requirement for PIP_2 is ancient and was present in Shaker family channels at roughly the time the KCNQ family first appeared. Thus, it is possible that KCNQ channels gained strict PIP_2 dependence de novo. It would be interesting to see if de novo insertion of single or a few basic residues within the gating machinery of diverse PIP_2-agnostic voltage-gated channels could awaken a latent PIP_2 sensitivity.

It remains to be seen if bimodal PIP_2 modulation is a conserved property of Elk channels, but the basic residues we identified as being important for PIP_2 modulation in Elk1 (K5, R347, and R479) are universally conserved as basic residues in mouse, human, fly, and sea anemone Elk channels, with one major exception (Fig. 8). The *Nematostella vectensis* (sea anemone) Elk orthologue lacks a basic residue at the 479 position, but it does have an adjacent R (at the 480 position equivalent) that is found in all Elk channels except Elk1. Erg1 is not modulated by PIP_2 in a bimodal fashion (Bian et al., 2001; Rodriguez et al., 2010) and like all Erg and Eag subfamily channels intriguingly lacks a basic residue at the equivalent position of R479 (Fig. 8 B). PIP_2 modulation has not been studied in the Eag subfamily to our knowledge, but it seems unlikely that they would have PIP_2-dependent mode shift given their evolutionarily conserved rapid deactivation (Li et al., 2015b). Thus, it appears that PIP_2 will have highly variable effects within the EAG family of channels. The auxiliary subunit KCNE1 enhances the PIP_2 sensitivity of KCNQ1, suggesting that PIP_2 modulation of EAG family channels could be further influenced by KCNEs, which are known to interact with some Erg and Elk channels (McDonald et al., 1997; Abbott et al., 1999; Clancy et al., 2009).

The position of the Cap domain in EAG family channels is somewhat controversial, with functional data from Eag1 (Terlau et al., 1997) and cross-linking experiments in Erg1 (de la Peña et al., 2011, 2015) suggesting close proximity to the S4–S5 linker, and structural and FRET data presenting an alternative that the Cap might instead interact through the CNBHD (Gianulis et al., 2013; Haitin et al., 2013). Structural evidence clearly shows the eag domain including part of the cap docks on the CNBHD (Haitin et al., 2013), but the complete position of the Cap has not been structurally resolved. However, it has been suggested that the Cap could regulate the S4–S5 linker while the eag domain is docked on the CNBHD (Gustina and Trudeau, 2012), and we find that the highly conserved basic residue near the tip of the Cap (K5 in Elk1) and R347 in the S4–S5 linker are both important for PIP_2-dependent mode shift. However, K5 could allosterically influence voltage gating through the eag domain, which we find is required for mode shift (Fig. 6). Basic residues R4 and R5 in the Cap of hErg1 are required for slow deactivation (Muskett et al., 2011) and the hErg1 Cap is required for mode shift (Tan et al., 2012), but the dependence of this effect on PIP_2 has not been explored. PIP_2 does appear to enhance hErg1 through open-state stabilization (Rodriguez et al., 2010), but currently only the distal C terminus of hErg1 has been linked to PIP_2-depenent modulation (Bian et al., 2004; Bian and McDonald, 2007).

The in vivo role of Elk channels has not been extensively studied, so the physiological importance of PIP_2-dependent modulation of Elk voltage gating is not yet clear. However, two of our findings suggest a possible role for PIP_2 in Elk1 modulation in vivo: (1) the Elk1 PIP_2 affinity is relatively low (Fig. 3), indicating that channel activity could be affected by physiological changes in PIP_2 (Suh and Hille, 2008); and (2) depletion of native PIP_2 with CiVSP in oocytes was sufficient to alter Elk1 gating properties (Fig. 4). Gene knockout and pharmacological experiments in mouse show that Elk2 in pyramidal neurons contributes to subthreshold K^+ conductance and alters firing threshold (Zhang et al., 2010). This is a qualitatively similar role to that played by KCNQ channels (M current), which strictly require PIP_2 for opening (Li et al., 2005; Zaydman et al., 2013; Zaydman and Cui, 2014). Elk1 current has not been identified in vivo, but it also activates at subthreshold potentials, is highly expressed in sympathetic ganglia (Shi et al., 1998), and is present at modest levels in various brain regions (Engeland et al., 1998; Zou et al., 2003). Our results suggest that the physiological roles of Elk and KCNQ channels fundamentally diverge at the level of PIP_2 regulation. Elk1 still activates after PIP_2 depletion, and the net effect of bimodal PIP_2 regulation

is inhibitory. PIP$_2$ serves to slow both the activation and deactivation rates of Elk1, which might effectively reduce the channel's response to rapid voltage changes. PIP$_2$ hydrolysis might then increase the response of the channel to brief depolarizations (accelerated activation) without a lasting increase in resting K$^+$ conductance (accelerated deactivation). Characterization of Elk1 currents in neurons with genetic and pharmacologic tools will be necessary to test these hypotheses.

REFERENCES

Abbott, G.W., F. Sesti, I. Splawski, M.E. Buck, M.H. Lehmann, K.W. Timothy, M.T. Keating, and S.A. Goldstein. 1999. MiRP1 forms IKr potassium channels with HERG and is associated with cardiac arrhythmia. *Cell.* 97:175–187. http://dx.doi.org/10.1016/S0092-8674(00)80728-X

Alonso-Ron, C., P. de la Peña, P. Miranda, P. Domínguez, and F. Barros. 2008. Thermodynamic and kinetic properties of aminoterminal and S4-S5 loop HERG channel mutants under steadystate conditions. *Biophys. J.* 94:3893–3911. http://dx.doi.org/10.1529/biophysj.107.116731

Bian, J.S., and T.V. McDonald. 2007. Phosphatidylinositol 4,5-bisphosphate interactions with the HERG K$^+$ channel. *Pflugers Arch.* 455:105–113. http://dx.doi.org/10.1007/s00424-007-0292-5

Bian, J., J. Cui, and T.V. McDonald. 2001. HERG K$^+$ channel activity is regulated by changes in phosphatidyl inositol 4,5-bisphosphate. *Circ. Res.* 89:1168–1176. http://dx.doi.org/10.1161/hh2401.101375

Bian, J.S., A. Kagan, and T.V. McDonald. 2004. Molecular analysis of PIP2 regulation of HERG and IKr. *Am. J. Physiol. Heart Circ. Physiol.* 287:H2154–H2163. http://dx.doi.org/10.1152/ajpheart.00120.2004

Brady, J.D., E.D. Rich, J.R. Martens, J.W. Karpen, M.D. Varnum, and R.L. Brown. 2006. Interplay between PIP3 and calmodulin regulation of olfactory cyclic nucleotide-gated channels. *Proc. Natl. Acad. Sci. USA.* 103:15635–15640. http://dx.doi.org/10.1073/pnas.0603344103

Brams, M., J. Kusch, R. Spurny, K. Benndorf, and C. Ulens. 2014. Family of prokaryote cyclic nucleotide-modulated ion channels. *Proc. Natl. Acad. Sci. USA.* 111:7855–7860. http://dx.doi.org/10.1073/pnas.1401917111

Brelidze, T.I., A.E. Carlson, and W.N. Zagotta. 2009. Absence of direct cyclic nucleotide modulation of mEAG1 and hERG1 channels revealed with fluorescence and electrophysiological methods. *J. Biol. Chem.* 284:27989–27997. http://dx.doi.org/10.1074/jbc.M109.016337

Brelidze, T.I., A.E. Carlson, B. Sankaran, and W.N. Zagotta. 2012. Structure of the carboxy-terminal region of a KCNH channel. *Nature.* 481:530–533. http://dx.doi.org/10.1038/nature10735

Brelidze, T.I., E.C. Gianulis, F. DiMaio, M.C. Trudeau, and W.N. Zagotta. 2013. Structure of the C-terminal region of an ERG channel and functional implications. *Proc. Natl. Acad. Sci. USA.* 110:11648–11653. http://dx.doi.org/10.1073/pnas.1306887110

Bright, S.R., E.D. Rich, and M.D. Varnum. 2007. Regulation of human cone cyclic nucleotide-gated channels by endogenous phospholipids and exogenously applied phosphatidylinositol 3,4,5-trisphosphate. *Mol. Pharmacol.* 71:176–183. http://dx.doi.org/10.1124/mol.106.026401

Chen, J., J.S. Mitcheson, M. Tristani-Firouzi, M. Lin, and M.C. Sanguinetti. 2001. The S4-S5 linker couples voltage sensing and activation of pacemaker channels. *Proc. Natl. Acad. Sci. USA.* 98:11277–11282. http://dx.doi.org/10.1073/pnas.201250598

Clancy, S.M., B. Chen, F. Bertaso, J. Mamet, and T. Jegla. 2009. KCNE1 and KCNE3 beta-subunits regulate membrane surface expression of Kv12.2 K$^+$ channels in vitro and form a tripartite complex in vivo. *PLoS One.* 4:e6330. http://dx.doi.org/10.1371/journal.pone.0006330

Craven, K.B., and W.N. Zagotta. 2006. CNG and HCN channels: Two peas, one pod. *Annu. Rev. Physiol.* 68:375–401. http://dx.doi.org/10.1146/annurev.physiol.68.040104.134728

Dai, G., C. Peng, C. Liu, and M.D. Varnum. 2013. Two structural components in CNGA3 support regulation of cone CNG channels by phosphoinositides. *J. Gen. Physiol.* 141:413–430. http://dx.doi.org/10.1085/jgp.201210944

Decher, N., J. Chen, and M.C. Sanguinetti. 2004. Voltage-dependent gating of hyperpolarization-activated, cyclic nucleotide-gated pacemaker channels: molecular coupling between the S4-S5 and C-linkers. *J. Biol. Chem.* 279:13859–13865. http://dx.doi.org/10.1074/jbc.M313704200

de la Peña, P., C. Alonso-Ron, A. Machín, J. Fernández-Trillo, L. Carretero, P. Domínguez, and F. Barros. 2011. Demonstration of physical proximity between the N terminus and the S4-S5 linker of the human ether-a-go-go-related gene (hERG) potassium channel. *J. Biol. Chem.* 286:19065–19075. http://dx.doi.org/10.1074/jbc.M111.238899

de la Peña, P., A. Machín, J. Fernández-Trillo, P. Domínguez, and F. Barros. 2015. Interactions between the N-terminal tail and the gating machinery of hERG K$^+$ channels both in closed and open/inactive states. *Pflugers Arch.* 467:1747–1756. http://dx.doi.org/10.1007/s00424-014-1612-1

Engeland, B., A. Neu, J. Ludwig, J. Roeper, and O. Pongs. 1998. Cloning and functional expression of rat ether-à-go-go-like K$^+$ channel genes. *J. Physiol.* 513:647–654. http://dx.doi.org/10.1111/j.1469-7793.1998.647ba.x

Flynn, G.E., and W.N. Zagotta. 2011. Molecular mechanism underlying phosphatidylinositol 4,5-bisphosphate-induced inhibition of SpIH channels. *J. Biol. Chem.* 286:15535–15542. http://dx.doi.org/10.1074/jbc.M110.214650

Ganetzky, B., G.A. Robertson, G.F. Wilson, M.C. Trudeau, and S.A. Titus. 1999. The eag family of K$^+$ channels in *Drosophila* and mammals. *Ann. NY Acad. Sci.* 868:356–369. http://dx.doi.org/10.1111/j.1749-6632.1999.tb11297.x

Gianulis, E.C., Q. Liu, and M.C. Trudeau. 2013. Direct interaction of eag domains and cyclic nucleotide–binding homology domains regulate deactivation gating in hERG channels. *J. Gen. Physiol.* 142:351–366. http://dx.doi.org/10.1085/jgp.201310995

Goodchild, S.J., L.C. Macdonald, and D. Fedida. 2015. Sequence of gating charge movement and pore gating in HERG activation and deactivation pathways. *Biophys. J.* 108:1435–1447. http://dx.doi.org/10.1016/j.bpj.2015.02.014

Gustina, A.S., and M.C. Trudeau. 2012. HERG potassium channel regulation by the N-terminal eag domain. *Cell. Signal.* 24:1592–1598. http://dx.doi.org/10.1016/j.cellsig.2012.04.004

Haitin, Y., A.E. Carlson, and W.N. Zagotta. 2013. The structural mechanism of KCNH-channel regulation by the eag domain. *Nature.* 501:444–448. http://dx.doi.org/10.1038/nature12487

Halaszovich, C.R., D.N. Schreiber, and D. Oliver. 2009. Ci-VSP is a depolarization-activated phosphatidylinositol-4,5-bisphosphate and phosphatidylinositol-3,4,5-trisphosphate 5′-phosphatase.

J. Biol. Chem. 284:2106–2113. http://dx.doi.org/10.1074/jbc.M803543200

Hilgemann, D.W. 2012. Fitting K_V potassium channels into the PIP_2 puzzle: Hille group connects dots between illustrious HH groups. *J. Gen. Physiol.* 140:245–248. http://dx.doi.org/10.1085/jgp.201210874

Hilgemann, D.W., S. Feng, and C. Nasuhoglu. 2001. The complex and intriguing lives of PIP2 with ion channels and transporters. *Sci. STKE.* 2001:re19.

Hull, C.M., S. Sokolov, A.C. Van Slyke, and T.W. Claydon. 2014. Regional flexibility in the S4-S5 linker regulates hERG channel closed-state stabilization. *Pflugers Arch.* 466:1911–1919. http://dx.doi.org/10.1007/s00424-013-1431-9

Jegla, T., and L. Salkoff. 1994. Molecular evolution of K^+ channels in primitive eukaryotes. *Soc. Gen. Physiol. Ser.* 49:213–222.

Jegla, T., and L. Salkoff. 1995. A multigene family of novel K^+ channels from *Paramecium tetraurelia. Receptors Channels.* 3:51–60.

Jegla, T., and L. Salkoff. 1997. A novel subunit for shal K^+ channels radically alters activation and inactivation. *J. Neurosci.* 17:32–44.

Jegla, T.J., C.M. Zmasek, S. Batalov, and S.K. Nayak. 2009. Evolution of the human ion channel set. *Comb. Chem. High Throughput Screen.* 12:2–23. http://dx.doi.org/10.2174/138620709787047957

Jegla, T., H.Q. Marlow, B. Chen, D.K. Simmons, S.M. Jacobo, and M.Q. Martindale. 2012. Expanded functional diversity of shaker K^+ channels in cnidarians is driven by gene expansion. *PLoS One.* 7:e51366. http://dx.doi.org/10.1371/journal.pone.0051366

Keating, M.T., and M.C. Sanguinetti. 2001. Molecular and cellular mechanisms of cardiac arrhythmias. *Cell.* 104:569–580. http://dx.doi.org/10.1016/S0092-8674(01)00243-4

Kruse, M., and B. Hille. 2013. The phosphoinositide sensitivity of the K_v channel family. *Channels (Austin).* 7:530–536. http://dx.doi.org/10.4161/chan.25816

Kruse, M., G.R. Hammond, and B. Hille. 2012. Regulation of voltage-gated potassium channels by $PI(4,5)P_2$. *J. Gen. Physiol.* 140:189–205. http://dx.doi.org/10.1085/jgp.201210806

Li, X., H. Liu, J. Chu Luo, S.A. Rhodes, L.M. Trigg, D.B. van Rossum, A. Anishkin, F.H. Diatta, J.K. Sassic, D.K. Simmons, et al. 2015a. Major diversification of voltage-gated K^+ channels occurred in ancestral parahoxozoans. *Proc. Natl. Acad. Sci. USA.* 112:E1010–E1019. http://dx.doi.org/10.1073/pnas.1422941112

Li, X., A.S. Martinson, M.J. Layden, F.H. Diatta, A.P. Sberna, D.K. Simmons, M.Q. Martindale, and T.J. Jegla. 2015b. Ether-à-go-go family voltage-gated K^+ channels evolved in an ancestral metazoan and functionally diversified in a cnidarian-bilaterian ancestor. *J. Exp. Biol.* 218:526–536. http://dx.doi.org/10.1242/jeb.110080

Li, Y., N. Gamper, D.W. Hilgemann, and M.S. Shapiro. 2005. Regulation of Kv7 (KCNQ) K^+ channel open probability by phosphatidylinositol 4,5-bisphosphate. *J. Neurosci.* 25:9825–9835. http://dx.doi.org/10.1523/JNEUROSCI.2597-05.2005

Long, S.B., E.B. Campbell, and R. Mackinnon. 2005a. Crystal structure of a mammalian voltage-dependent Shaker family K^+ channel. *Science.* 309:897–903. http://dx.doi.org/10.1126/science.1116269

Long, S.B., E.B. Campbell, and R. Mackinnon. 2005b. Voltage sensor of Kv1.2: Structural basis of electromechanical coupling. *Science.* 309:903–908. http://dx.doi.org/10.1126/science.1116270

Martinson, A.S., D.B. van Rossum, F.H. Diatta, M.J. Layden, S.A. Rhodes, M.Q. Martindale, and T. Jegla. 2014. Functional evolution of Erg potassium channel gating reveals an ancient origin for IKr. *Proc. Natl. Acad. Sci. USA.* 111:5712–5717. http://dx.doi.org/10.1073/pnas.1321716111

McDonald, T.V., Z. Yu, Z. Ming, E. Palma, M.B. Meyers, K.W. Wang, S.A. Goldstein, and G.I. Fishman. 1997. A minK-HERG complex regulates the cardiac potassium current I(Kr). *Nature.* 388:289–292. http://dx.doi.org/10.1038/40882

Morais Cabral, J.H., A. Lee, S.L. Cohen, B.T. Chait, M. Li, and R. Mackinnon. 1998. Crystal structure and functional analysis of the HERG potassium channel N terminus: A eukaryotic PAS domain. *Cell.* 95:649–655. http://dx.doi.org/10.1016/S0092-8674(00)81635-9

Murata, Y., H. Iwasaki, M. Sasaki, K. Inaba, and Y. Okamura. 2005. Phosphoinositide phosphatase activity coupled to an intrinsic voltage sensor. *Nature.* 435:1239–1243. http://dx.doi.org/10.1038/nature03650

Muskett, F.W., S. Thouta, S.J. Thomson, A. Bowen, P.J. Stansfeld, and J.S. Mitcheson. 2011. Mechanistic insight into human ether-à-go-go-related gene (hERG) K^+ channel deactivation gating from the solution structure of the EAG domain. *J. Biol. Chem.* 286:6184–6191. http://dx.doi.org/10.1074/jbc.M110.199364

Peters, H.C., H. Hu, O. Pongs, J.F. Storm, and D. Isbrandt. 2005. Conditional transgenic suppression of M channels in mouse brain reveals functions in neuronal excitability, resonance and behavior. *Nat. Neurosci.* 8:51–60. http://dx.doi.org/10.1038/nn1375

Piper, D.R., A. Varghese, M.C. Sanguinetti, and M. Tristani-Firouzi. 2003. Gating currents associated with intramembrane charge displacement in HERG potassium channels. *Proc. Natl. Acad. Sci. USA.* 100:10534–10539. http://dx.doi.org/10.1073/pnas.1832721100

Poblete, H., I. Oyarzún, P. Olivero, J. Comer, M. Zuñiga, R.V. Sepulveda, D. Báez-Nieto, C. González Leon, F. González-Nilo, and R. Latorre. 2015. Molecular determinants of phosphatidylinositol 4,5-bisphosphate (PI(4,5)P2) binding to transient receptor potential V1 (TRPV1) channels. *J. Biol. Chem.* 290:2086–2098. http://dx.doi.org/10.1074/jbc.M114.613620

Rodriguez, N., M.Y. Amarouch, J. Montnach, J. Piron, A.J. Labro, F. Charpentier, J. Mérot, I. Baró, and G. Loussouarn. 2010. Phosphatidylinositol-4,5-bisphosphate (PIP(2)) stabilizes the open pore conformation of the Kv11.1 (hERG) channel. *Biophys. J.* 99:1110–1118. http://dx.doi.org/10.1016/j.bpj.2010.06.013

Rodriguez-Menchaca, A.A., S.K. Adney, Q.Y. Tang, X.Y. Meng, A. Rosenhouse-Dantsker, M. Cui, and D.E. Logothetis. 2012a. PIP2 controls voltage-sensor movement and pore opening of Kv channels through the S4-S5 linker. *Proc. Natl. Acad. Sci. USA.* 109:E2399–E2408. http://dx.doi.org/10.1073/pnas.1207901109

Rodríguez-Menchaca, A.A., S.K. Adney, L. Zhou, and D.E. Logothetis. 2012b. Dual regulation of voltage-sensitive ion channels by PIP(2). *Front. Pharmacol.* 3:170. http://dx.doi.org/10.3389/fphar.2012.00170

Rohács, T., C.M. Lopes, I. Michailidis, and D.E. Logothetis. 2005. PI(4,5)P2 regulates the activation and desensitization of TRPM8 channels through the TRP domain. *Nat. Neurosci.* 8:626–634. http://dx.doi.org/10.1038/nn1451

Sanguinetti, M.C., C. Jiang, M.E. Curran, and M.T. Keating. 1995. A mechanistic link between an inherited and an acquired cardiac arrhythmia: HERG encodes the I_{Kr} potassium channel. *Cell.* 81:299–307. http://dx.doi.org/10.1016/0092-8674(95)90340-2

Schachtman, D.P., J.I. Schroeder, W.J. Lucas, J.A. Anderson, and R.F. Gaber. 1992. Expression of an inward-rectifying potassium channel by the Arabidopsis KAT1 cDNA. *Science.* 258:1654–1658. http://dx.doi.org/10.1126/science.8966547

Sentenac, H., N. Bonneaud, M. Minet, F. Lacroute, J.M. Salmon, F. Gaymard, and C. Grignon. 1992. Cloning and expression in yeast of a plant potassium ion transport system. *Science.* 256:663–665. http://dx.doi.org/10.1126/science.1585180

Shi, W., H.S. Wang, Z. Pan, R.S. Wymore, I.S. Cohen, D. McKinnon, and J.E. Dixon. 1998. Cloning of a mammalian elk potassium channel gene and EAG mRNA distribution in rat sympathetic ganglia. *J. Physiol.* 511:675–682. http://dx.doi.org/10.1111/j.1469-7793.1998.675bg.x

Suh, B.C., and B. Hille. 2008. PIP_2 is a necessary cofactor for ion channel function: How and why? *Annu. Rev. Biophys.* 37:175–195. http://dx.doi.org/10.1146/annurev.biophys.37.032807.125859

Suh, B.C., K. Leal, and B. Hille. 2010. Modulation of high-voltage activated Ca^{2+} channels by membrane phosphatidylinositol 4,5-bisphosphate. *Neuron.* 67:224–238. http://dx.doi.org/10.1016/j.neuron.2010.07.001

Tan, P.S., M.D. Perry, C.A. Ng, J.I. Vandenberg, and A.P. Hill. 2012. Voltage-sensing domain mode shift is coupled to the activation gate by the N-terminal tail of hERG channels. *J. Gen. Physiol.* 140:293–306. http://dx.doi.org/10.1085/jgp.201110761

Terlau, H., S.H. Heinemann, W. Stühmer, O. Pongs, and J. Ludwig. 1997. Amino terminal-dependent gating of the potassium channel rat eag is compensated by a mutation in the S4 segment. *J. Physiol.* 502:537–543. http://dx.doi.org/10.1111/j.1469-7793.1997.537bj.x

Tristani-Firouzi, M., J. Chen, and M.C. Sanguinetti. 2002. Interactions between S4-S5 linker and S6 transmembrane domain modulate gating of HERG K^+ channels. *J. Biol. Chem.* 277:18994–19000. http://dx.doi.org/10.1074/jbc.M200410200

Trudeau, M.C., J.W. Warmke, B. Ganetzky, and G.A. Robertson. 1995. HERG, a human inward rectifier in the voltage-gated potassium channel family. *Science.* 269:92–95. http://dx.doi.org/10.1126/science.7604285

Trudeau, M.C., S.A. Titus, J.L. Branchaw, B. Ganetzky, and G.A. Robertson. 1999. Functional analysis of a mouse brain Elk-type K^+ channel. *J. Neurosci.* 19:2906–2918.

Vanhaesebroeck, B., S.J. Leevers, K. Ahmadi, J. Timms, R. Katso, P.C. Driscoll, R. Woscholski, P.J. Parker, and M.D. Waterfield. 2001. Synthesis and function of 3-phosphorylated inositol lipids. *Annu. Rev. Biochem.* 70:535–602. http://dx.doi.org/10.1146/annurev.biochem.70.1.535

Villalba-Galea, C.A., W. Sandtner, D.M. Starace, and F. Bezanilla. 2008. S4-based voltage sensors have three major conformations. *Proc. Natl. Acad. Sci. USA.* 105:17600–17607. http://dx.doi.org/10.1073/pnas.0807387105

Wang, J., M.C. Trudeau, A.M. Zappia, and G.A. Robertson. 1998. Regulation of deactivation by an amino terminal domain in human ether-à-go-go–related gene potassium channels. *J. Gen. Physiol.* 112:637–647. http://dx.doi.org/10.1085/jgp.112.5.637

Warmke, J.W., and B. Ganetzky. 1994. A family of potassium channel genes related to eag in Drosophila and mammals. *Proc.* *Natl. Acad. Sci. USA.* 91:3438–3442. http://dx.doi.org/10.1073/pnas.91.8.3438

Womack, K.B., S.E. Gordon, F. He, T.G. Wensel, C.C. Lu, and D.W. Hilgemann. 2000. Do phosphatidylinositides modulate vertebrate phototransduction? *J. Neurosci.* 20:2792–2799.

Wu, L., C.S. Bauer, X.G. Zhen, C. Xie, and J. Yang. 2002. Dual regulation of voltage-gated calcium channels by PtdIns(4,5)P2. *Nature.* 419:947–952. http://dx.doi.org/10.1038/nature01118

Yu, F.H., and W.A. Catterall. 2004. The VGL-chanome: A protein superfamily specialized for electrical signaling and ionic homeostasis. *Sci. STKE.* 2004:re15.

Zaydman, M.A., and J. Cui. 2014. PIP_2 regulation of KCNQ channels: biophysical and molecular mechanisms for lipid modulation of voltage-dependent gating. *Front. Physiol.* 5:195. http://dx.doi.org/10.3389/fphys.2014.00195

Zaydman, M.A., J.R. Silva, K. Delaloye, Y. Li, H. Liang, H.P. Larsson, J. Shi, and J. Cui. 2013. Kv7.1 ion channels require a lipid to couple voltage sensing to pore opening. *Proc. Natl. Acad. Sci. USA.* 110:13180–13185. http://dx.doi.org/10.1073/pnas.1305167110

Zhainazarov, A.B., M. Spehr, C.H. Wetzel, H. Hatt, and B.W. Ache. 2004. Modulation of the olfactory CNG channel by PtdIns(3,4,5)P3. *J. Membr. Biol.* 201:51–57. http://dx.doi.org/10.1007/s00232-004-0707-4

Zhang, X., F. Bertaso, J.W. Yoo, K. Baumgärtel, S.M. Clancy, V. Lee, C. Cienfuegos, C. Wilmot, J. Avis, T. Hunyh, et al. 2010. Deletion of the potassium channel Kv12.2 causes hippocampal hyperexcitability and epilepsy. *Nat. Neurosci.* 13:1056–1058. http://dx.doi.org/10.1038/nn.2610

Zhen, X.G., C. Xie, Y. Yamada, Y. Zhang, C. Doyle, and J. Yang. 2006. A single amino acid mutation attenuates rundown of voltage-gated calcium channels. *FEBS Lett.* 580:5733–5738. http://dx.doi.org/10.1016/j.febslet.2006.09.027

Zhou, L., and D.E. Logothetis. 2013. The where and how of PIP regulation of cone photoreceptor CNG channels. *J. Gen. Physiol.* 141:403–407. http://dx.doi.org/10.1085/jgp.201310981

Zou, A., Z. Lin, M. Humble, C.D. Creech, P.K. Wagoner, D. Krafte, T.J. Jegla, and A.D. Wickenden. 2003. Distribution and functional properties of human KCNH8 (Elk1) potassium channels. *Am. J. Physiol. Cell Physiol.* 285:C1356–C1366. http://dx.doi.org/10.1152/ajpcell.00179.2003